

Eu(III) Complex with DO3A-amino-phosphonate Ligand as a Concentration-Independent pH-Responsive Contrast Agent for Magnetic Resonance Spectroscopy (MRS)

Tereza Krchová,[†] Vít Herynek,[‡] Andrea Gálisová,[‡] Jan Blahut,[†] Petr Hermann,[†] and Jan Kotek^{*,†} 

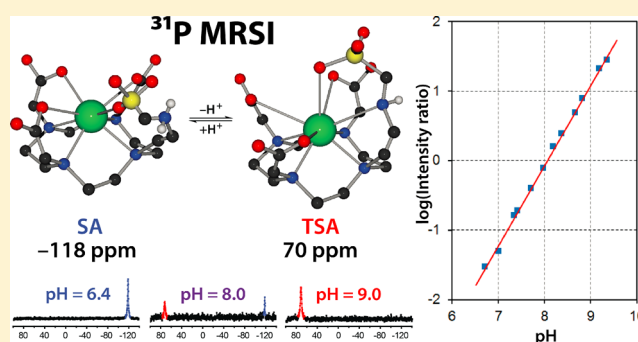
[†]Department of Inorganic Chemistry, Faculty of Science, Charles University, Hlavova 2030, Prague 2 128 43, Czech Republic

[‡]Department of Radiodiagnostic and Interventional Radiology, Magnetic Resonance Unit, Institute for Clinical and Experimental Medicine, Vídeňská 1958/9, Prague 4 140 21, Czech Republic

Supporting Information

ABSTRACT: A new DOTA-like ligand H₅do3aNP with a 2-[amino(methylphosphonic acid)]ethyl-coordinating pendant arm was prepared, and its coordinating properties were studied by NMR spectroscopy and potentiometry. The study revealed a rare slow exchange (on the ¹H and ³¹P NMR time scale) between protonated and unprotonated complex species with a corresponding acidity constant pK_A ~ 8.0. This unusually slow time scale associated with protonation is caused by a significant geometric change from square-antiprismatic (SA) arrangement observed for protonated complex SA-[Eu(Hdo3aNP)]⁻ to twisted-square-antiprismatic (TSA) arrangement found for deprotonated complex TSA-[Eu(do3aNP)]²⁻. This behavior

results in simultaneous occurrence of the signals of both species in the ³¹P NMR spectra at approximately -118 and +70 ppm, respectively. Such an unprecedented difference in the chemical shifts between species differing by a proton is caused by a significant movement of the principal magnetic axis and by a change of phosphorus atom position in the coordination sphere of the central Eu(III) ion (i.e., by relative movement of the phosphorus atom with respect to the principal magnetic axis). It changes the sign of the paramagnetic contribution to the ³¹P NMR chemical shift. The properties discovered can be employed in the measurement of pH by MRS techniques as presented by proof-of-principle experiments on phantoms.



■ INTRODUCTION

Over the past two decades, the ability to provide essential information about variations in tissue pH has become increasingly important. Therefore, it is not surprising that magnetic resonance imaging (MRI), as one of the most widely used diagnostic methods in clinical medicine,¹ has been proposed as a suitable technique for this purpose. The tumor extracellular microenvironment is often slightly more acidic than healthy tissue due to increased anaerobic glycolysis and a related accumulation of lactic acid, reduced passive buffering capacity, and poor tissue perfusion.² For example, the extracellular pH in solid tumors typically ranges between 6.5 and 7.2.³ Therefore, measurement of extracellular pH using noninvasive techniques is important not only for early detection of disease or metabolic disorder, but also for suggesting the most efficient treatment and for monitoring the effects of pH-altering therapies.² Nowadays, several strategies (and appropriate contrast agents, CAs) to measure tissue pH are intensively investigated.⁴ Previous studies have suggested relaxation-based MRI CAs with longitudinal relaxivity (*r*₁) dependent on pH.⁵ The Gd(III) complexes investigated were based on a variation in the number of inner-sphere water molecules (*q*), for example, caused by the

presence of β -arylsulfonamide⁶ or *p*-nitrophenol⁷ groups on the chelate species. The deprotonation and coordination of these groups is associated with removal of the inner-sphere water molecule, and such a change in *q* leads to a change in relaxivity *r*₁. Similarly, in the case of Gd(III) complexes of H₃do3a with 2-aminoethyl pendant arms, such as H₃do3a-ae (Figure 1), a change in the protonation state of the amino group causes a (de)coordination of the pendant arm, and thus, it also leads to changes in relaxivity.⁸ Interesting results have been obtained by Hall et al., who studied the Gd(III) complex with terpyridine-containing macrocycle.⁹ The authors demonstrated a significant decrease of relaxivity with increasing pH and attributed it to a decrease in *q* from 3 to 0 due to formation of the hydroxido species and hydroxido-bridged dimer connected with a negligible exchange rate of coordinated OH⁻ ions.⁹ However, for quantification of pH using these relaxation-based CAs, knowledge of the actual agent concentration is needed.¹⁰ This is the reason why new methods employing ratiometric approaches are developed, as they remove dependence of the observed signal on the local concentration of CAs. For example,

Received: November 17, 2016

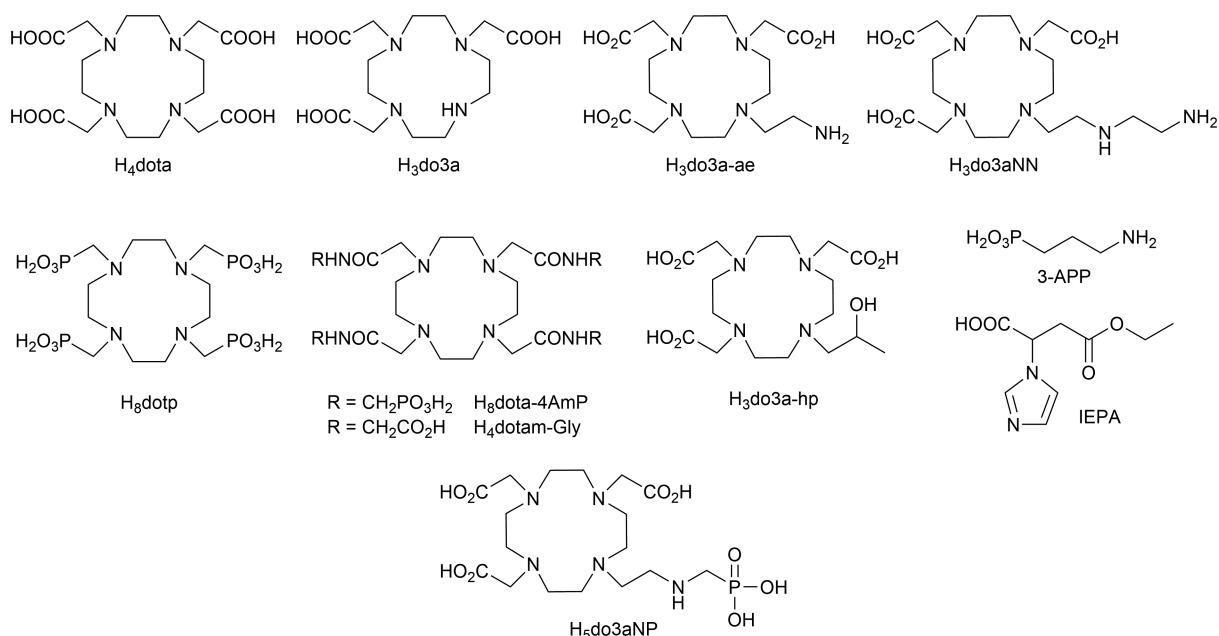


Figure 1. Structural formulas of the ligands discussed in the text.

Gillies and co-workers developed a “dual-injection” relaxivity-based method employing administration of two compounds (pH-sensitive $[\text{Gd}(\text{dota-4AmP})]^{5-}$ and pH-insensitive $[\text{Gd}(\text{dotp})]^{5-}$; for structures of both ligands, see Figure 1) with a comparable biodistribution and pharmacokinetics, allowing determination of the concentration of the first agent from the concentration of the second one. It was shown that this approach allowed pH mapping both *in vitro* and *in vivo*.^{5b,10,11} An alternative approach was introduced by Aime et al. They investigated the possibility of measuring the ratio of transversal and longitudinal relaxation rates of water protons (R_2/R_1) after injecting a single paramagnetic Gd(III) complex of DOTA-functionalized polypeptide (poly-L-ornithine).¹² Recently, the paramagnetic MRI contrast agents that are detected via the chemical exchange saturation transfer (CEST) effect, so-called PARACEST CAs, have also been used to ratiometrically estimate *in vitro/in vivo* pH by utilizing a ratio of two different CEST signals.^{3,13} These can originate from the exchangeable protons of the same molecule, as in the case of paramagnetic $\text{H}_4\text{dotam-Gly}$ (Figure 1) complexes with some Ln(III) ions (Pr, Nd, and Eu) where the protons of a coordinated water molecule and amide protons of the macrocyclic ligand represent two CEST-active exchanging pools.¹⁴ Similarly, the Yb(III) complex of $\text{H}_3\text{do3aNN}$ (Figure 1) with two proton-exchanging pools of the primary and secondary amino groups has been shown to be suitable for this purpose.¹⁵ Two different CEST signals can also originate from two conformations of the same molecule generating CEST signals at different chemical shifts, as was shown for Yb(III)-analogue of the clinically used $[\text{Gd}(\text{do3a-hp})(\text{H}_2\text{O})]$ (ProHance; Figure 1).^{13e,16}

An alternative approach to *in vivo* pH measurement is the MRS (magnetic resonance spectroscopy) technique. In general, MRS provides information about abundance and concentration of tissue metabolites, and it can help to characterize many pathologies, including neurological, psychiatric, and metabolic diseases.¹⁷ In addition, spectral information on a metabolite/compound with a particular chemical shift can be encoded into the image, and a map of its spatial distribution can be reconstructed by a method called magnetic resonance

spectroscopic imaging (MRSI). Several methods for pH mapping by MRS using different endogenous or exogenous compounds have been used, and these are generally based on a difference in chemical shifts between pH-dependent and pH-independent resonances. Application of MRS to measure pH began early on with the acquisition of the ^{31}P MR spectra of inorganic phosphate (P_i) because its resonance frequency is pH-dependent. The majority of P_i resonance comes from intracellular phosphate,¹⁸ and thus, the chemical shift of the P_i generally reflects the intracellular pH.^{2,11,19} To determine the extracellular pH of tumors in animal models, nontoxic exogenous reporter 3-aminopropylphosphonic acid (3-APP; Figure 1) with chemical shift dependence ~ 1 ppm per pH unit has been used.^{2,19} Tissue pH can also be detected *in vivo* using diamagnetic ^1H MRS probes with the pH-sensitive signal of ^1H nucleus. Exogenously administered 2-imidazol-1-yl-3-ethoxycarbonyl-propionic acid (IEPA; Figure 1) has been employed for this purpose. The chemical shift of the imidazole ring C-2 hydrogen atom is in the 7–9 ppm range and is pH-sensitive. This compound has been used for imaging extracellular pH in breast or brain tumors.²⁰ However, the disadvantage of using diamagnetic compounds as pH probes is the fact that their signal can be overlapped with the resonances of other compounds present *in vivo*. Therefore, complexes of paramagnetic metal ions are studied due to the expanded chemical shift scale of NMR-active nuclei. In particular, Ln(III) complexes with macrocyclic ligands have been used because they are stable under *in vivo* conditions. The Yb(III) complex of H_8dotp (Figure 1) has been introduced as a prototype of a new class of pH indicators because stepwise protonation of the complex is accompanied by variations in the protons' chemical shifts (6 resonances in ^1H NMR spectrum); this enables creation of a calibration curve for pH determination.²¹ Simultaneous determination of pH and temperature by Tm(III) complexes of H_8dotp using three proton chemical shifts was studied by a three-dimensional chemical shift method called biosensor imaging of redundant deviation in shift (BIRDS).²² The Ln(III) complexes of two metal ions (Tm and Yb) with phosphonate ligand $\text{H}_8\text{dota-4AmP}$ (Figure 1)

also exhibit suitable pH-sensitivities for BIRDS detection using chemical shift difference between two proton resonances. Moreover, these agents are also CEST-active, and thus, the CEST effect observed together with BIRDS opens the way toward high-resolution and quantitative pH imaging.²³

To contribute to the fields described above, we prepared a new macrocyclic ligand H₃do3aNP (Figure 1). The amino-phosphonate-coordinating pendant arm was chosen because, in general, protonation constants of amino and phosphonate groups are close to the physiological pH; thus, the complexes of the new ligand were expected to change their properties in the pH region relevant for living systems. In addition, the presence of a phosphorus atom could be potentially employed in ³¹P NMR-based applications. In this work, we report on ligand synthesis and the unusual ¹H and ³¹P NMR properties of its europium(III) complex which are employable in ³¹P MRS/MRSI for determination of pH. In addition, potentiometric and NMR studies found high stability for the studied complex in solution, which is promising for potential *in vivo* use of related compounds.

EXPERIMENTAL SECTION

Materials and Methods. Unless stated otherwise, commercially available chemicals and solvents were used without further purification. Water used for potentiometric titrations was deionized by the Milli-Q device (Millipore).

1,4,7-Tris(*tert*-butylcarboxymethyl)-1,4,7,10-tetraazacyclododecane hydrobromide (tBu₃do3a-HBr)²⁴ and *N*-benzylethanolamine²⁵ were prepared according to the published procedures. Dichloromethane (DCM) was dried by the standard procedure²⁶ and stored over molecular sieves under an argon atmosphere.

NMR characterization data (1D: ¹H, ¹³C; 2D: HSQC, HMB, ¹H–¹H COSY, ¹H–¹H EXSY, ³¹P–³¹P EXSY) were recorded on VNMR300, Bruker Avance III 400, or Bruker Avance III 600 spectrometers, using 5 mm sample tubes. The longitudinal relaxation times *T*₁'s of ³¹P were measured on the VNMR300 by inversion recovery pulse sequence (15 or 10 increments on d2 exponentially sampled) with the spectrometer offset identical to the compound signal and properly calibrated pulse length. Selectively ¹H-decoupled ¹³C NMR spectra were obtained on the Bruker Avance III 600 spectrometer by standard one-pulse ¹³C measurement with low-power continuous-wave ¹H decoupling at the desired frequency offset. Exchange rates were measured using a selective ³¹P–³¹P EXSY pulse sequence with the mixing-time changing from 20 μs to 500 ms exponentially. Exchange rates of isomer interchange were determined by numerical fitting of the mixing-time-dependent ³¹P NMR integral value with the Bloch–McConnell equation using Matlab.²⁷ Unless stated otherwise, NMR experiments were performed at 25 °C. The pD value means a reading of the freshly calibrated pH electrode of the sample dissolved in D₂O corrected by +0.4. Chemical shifts δ are given in ppm, and coupling constants *J* are reported in Hz. For ¹H and ¹³C{¹H} measurements of diamagnetic compounds in D₂O, tBuOH was used as the internal standard (δ_H = 1.25, δ_C = 30.29). For the measurements in CDCl₃, TMS was used as the internal standard (δ_H = 0.00, δ_C = 0.00). For ³¹P measurements, 85% H₃PO₄ in H₂O was used as the external standard (δ_P = 0.00). In the case of paramagnetic complexes, ¹H chemical shifts were referenced to the tBuOH signal of the sample (δ_H = 1.25). Abbreviations [s (singlet), d (doublet), t (triplet), m (multiplet), and br (broad)] are used in order to express the signal multiplicities. Lanthanide(III) concentrations in solutions were determined by measuring bulk magnetic susceptibility (BMS) shifts.²⁸

The ESI-MS spectra were run on the Bruker ESQUIRE 3000 spectrometer equipped with an electrospray ion source and ion-trap detection. The measurements were carried out in both positive and negative modes.

Luminescence spectra were acquired on a Luminescence Thermo Spectronic spectrometer AMINCO Bowman Series 2. The luminescence spectra were obtained after excitation at the Eu(III) ⁵L₆ ← ⁷F₀ band (λ = 396 nm).

Syntheses. *Synthesis of 1.* Paraformaldehyde (4.00 g, 133 mmol) was added to a well-stirred solution of *N*-benzylethanolamine (4.00 g, 26.5 mmol) and diethyl-phosphite (17.2 mL, 134 mmol) in dry MeCN (30 mL). The reaction mixture was stirred at 60 °C for 2 days, filtered, and then evaporated on a rotary evaporator. The oily residue was dissolved in a small amount of EtOH, and then the solution was loaded onto a strong cation exchanger column (Dowex 50, H⁺-form, 4 cm × 20 cm, in EtOH). Impurities were removed by elution with EtOH, and product **1** was eluted with concentrated aqueous NH₃/EtOH (1/5). The fractions containing product **1** (TLC and ¹H NMR check) were combined, evaporated, redissolved in absolute EtOH, and evaporated to give compound **1** (7.62 g, 95.6%) as a brownish oil.

¹H NMR (299.9 MHz, CD₃OD): δ 1.34 (6H, t, ³J_{HH} = 7.0, CH₂CH₃); 2.80 (2H, t, ³J_{HH} = 6.0, CH₂CH₂OH); 3.07 (2H, d, ²J_{HP} = 10.0, PCH₂N); 3.67 (2H, t, ³J_{HH} = 6.0, CH₂CH₂OH); 3.85 (2H, s, CH₂Ph); 4.13 (4H, dq, ³J_{HH} = ³J_{PH} = 7.0, CH₂CH₃); 7.25–7.41 (5H, m, arom). ¹³C{¹H} NMR (75.4 MHz, CD₃OD): δ 17.64 (2C, d, ³J_{CP} = 6.0, OCH₂CH₃); 51.09 (1C, d, ¹J_{CP} = 162, PCH₂N); 58.89 (1C, d, ³J_{CP} = 8.0, CH₂); 61.9 (1C, CH₂); 62.24 (1C, ³J_{CP} = 7.5, CH₂); 64.39 (2C, ²J_{CP} = 7.0, OCH₂CH₃); 129.16 (1C, arom); 130.18 (2C, arom); 131.02 (2C, arom); 140.83 (1C, arom quaternary). ³¹P{¹H} NMR (121.4 MHz, CD₃OD): δ 27.17 (1P, s). ³¹P NMR (121.4 MHz, CD₃OD): δ 27.17 (1P, m). MS-ESI: (+) 323.7 ([M + Na]⁺, calcd 324.1).

Synthesis of 2. A solution of CH₃SO₂Cl (1.14 g, 9.96 mmol, 1.2 equiv) in dry CH₂Cl₂ (10 mL) was dropwise added to a well-stirred solution of **1** (2.50 g, 8.30 mmol) and Et₃N (1.68 g, 16.6 mmol, 2 equiv) in dry CH₂Cl₂ (70 mL) with cooling (ice bath). The reaction mixture was then stirred for 20 min. Next, saturated aqueous NaHCO₃ (50 mL) was added, and the mixture was stirred for 10 min. The organic layer was separated, washed with saturated aqueous NaHCO₃ (2 × 30 mL) and H₂O (2 × 30 mL), dried over Na₂SO₄, and concentrated *in vacuo* to give 3.05 g (97%) of **2** as a brownish oil. Compound **2** is not stable and must be immediately used for further synthesis.

¹H NMR (299.9 MHz, CDCl₃): δ 1.31 (6H, t, ³J_{HH} = 7.0, CH₂CH₃); 2.98 (2H, d, ²J_{HP} = 11.0, PCH₂N); 2.99 (3H, s, CH₃); 3.08 (2H, t, ³J_{HH} = 6.0, OCH₂CH₂N); 3.85 (2H, s, CH₂Ph); 4.09 (4H, dq, ³J_{HH} = ³J_{PH} = 7.0, CH₂CH₃); 4.29 (2H, t, ³J_{HH} = 6.0, S(O)₂CH₂CH₂N); 7.23–7.35 (5H, m, arom). ¹³C{¹H} NMR (75.4 MHz, CDCl₃): δ 16.60 (2C, d, ³J_{CP} = 6.0, OCH₂CH₃); 37.50 (1C, S(O)₂CH₃); 49.67 (1C, d, ¹J_{CP} = 159, PCH₂N); 53.62 (1C, d, ³J_{CP} = 6.0, CH₂); 60.40 (1C, ³J_{CP} = 9.0, CH₂); 62.03 (2C, ²J_{CP} = 7.0, OCH₂CH₃); 68.19 (1C, CH₂); 127.56 (1C, arom); 128.49 (2C, arom); 129.11 (2C, arom); 138.17 (1C, arom quaternary). ³¹P{¹H} NMR (121.4 MHz, CDCl₃): δ 24.80 (1P, s). ³¹P NMR (121.4 MHz, CDCl₃): δ 24.80 (1P, m).

Synthesis of 3. A solution of alkylating reagent **2** (2.71 g, 7.14 mmol, 1.70 equiv) in dry MeCN (30 mL) was dropwise added to a well-stirred suspension of tBu₃do3a-HBr (2.50 g, 4.20 mmol) and K₂CO₃ (1.15 g, 8.3 mmol, 2 equiv) in dry MeCN (45 mL). The reaction mixture was stirred at room temperature for 1 day and filtered, and the filtrate was evaporated on a rotary evaporator. The oily residue was dissolved in CHCl₃ (30 mL) and extracted with distilled water (4 × 15 mL). The organic layer was dried over Na₂SO₄ and concentrated *in vacuo* to give 4.50 g of a yellow oil containing crude compound **3** contaminated with an excess of the alkylating reagent **2** and the products of its degradation. Crude product **3** was used in the next step without purification.

³¹P{¹H} NMR (121.4 MHz, CDCl₃, 25 °C): δ 25.89 (1P, s). ³¹P NMR (121.4 MHz, CDCl₃): δ 25.89 (1P, m). MS-ESI: (+) 797.8 ([M + H]⁺, calcd 798.5); 819.9 ([M + Na]⁺, calcd 820.5).

Synthesis of 4. The total amount of crude compound **3** obtained above (4.50 g) was dissolved in a mixture of CF₃CO₂H and CHCl₃ (40 mL, 1:1 v:v). The resulting solution was refluxed for 18 h and then evaporated on a rotary evaporator. The oily residue was dissolved in a

small amount of distilled water and evaporated, and this procedure was repeated three more times. The oily residue was dissolved in a small amount of distilled water, and the solution was loaded onto a strong cation exchanger column (Dowex 50, H⁺-form, 4 cm × 15 cm). The impurities were removed by elution with water, and product 4 was eluted with aq NH₃ (5%). The fractions containing product 4 (¹H NMR check) were combined. After evaporation of volatiles, the oily residue was dissolved in water and poured onto a column of a weak cation exchanger (Amberlite CG50, 200–400 mesh, 4 cm × 15 cm). The impurities were eluted off with water, and product 4 was collected by 20% aq CH₃COOH. The fractions containing product 4 were combined and evaporated to give 2.30 g of brownish oil, which was used in the next step without further purification.

When crude product 4 prepared in another batch was left to stand for several days, it solidified on standing. The sample for elemental analysis was isolated by washing this solid with ethanol, filtering, and then equilibrating the solid in ambient air.

¹H NMR (600 MHz, D₂O, 50 °C, pD = 6.74, Figure S1): δ 1.33 (6H, t, ³J_{HH} = 7.0, CH₂CH₃); 2.94 (2H, t, ³J_{HH} = 6.0, CH₂NCH₂Ph); 3.01–3.85 (6H, br, CH₂CH₂NCH₂Ph + macrocyclic CH₂); 3.11–3.16 (6H, br, NCH₂P + macrocyclic CH₂); 3.18–3.22 (4H, br m, macrocyclic CH₂); 3.29–3.34 (4H, br m, macrocyclic CH₂); 3.45 (4H, br s, CH₂CO); 3.58 (2H, br s, CH₂CO); 3.81 (2H, s, NCH₂Ph); 4.14 (4H, m, CH₂CH₃); 7.38–7.47 (5H, m, arom). ¹³C{¹H} NMR (150.9 MHz, D₂O, 50 °C, pD = 6.74, Figure S2): δ 16.30 (2C, OCH₂CH₃); 49.69 (1C, d, ¹J_{CP} = 160, PCH₂N); 49.69 (1C, d, ³J_{CP} = 8.0, CH₂NCH₂Ph); 49.91 (2C, macrocyclic CH₂); 50.71 (2C, macrocyclic CH₂); 50.86 (1C, CH₂CH₂NCH₂Ph); 51.11 (4C, macrocyclic CH₂); 56.40 (1C, CH₂CO); 57.47 (2C, CH₂CO); 60.66 (1C, d, ³J_{CP} = 8.5, CH₂Ph); 64.22 (1C, d, ²J_{CP} = 6.5, OCH₂CH₃); 128.52 (1C, arom); 129.34 (2C, arom); 13.21 (2C, arom); 138.44 (1C, arom quaternary); 173.73 (1C, CH₂CO); 174.94 (2C, CH₂CO). ³¹P{¹H} NMR (121.4 MHz, D₂O, pD = 6.74, Figure S3): δ 28.39 (1P, s). ³¹P NMR (121.4 MHz, D₂O, pD = 6.74, Figure S4): δ 28.39 (1P, m). MS-ESI: (+) 629.3 ([M + H]⁺, calcd 630.0); 652.0 ([M + Na]⁺, calcd 652.3); (–) 627.8 ([M – H][–], calcd 628.3). Elemental analysis found (calcd for 4·4H₂O, C₂₈H₃₆N₅O₁₃P, M_r = 701.8): C, 47.90 (47.92); H, 7.54 (8.04); N, 9.76 (9.98); P, 3.94 (4.41).

Synthesis of 5. The total amount of crude product 4 obtained above (2.30 g) was dissolved in concentrated aqueous HCl (20 mL) and stirred at 95 °C for 24 h. Then, the solution was evaporated on a rotary evaporator, dissolved in a small amount of water, and loaded onto a strong cation exchanger column (Dowex 50, H⁺-form, 4 cm × 15 cm). The impurities were removed by elution with water, and product 5 was eluted with 5% aq NH₃. The fractions containing the product were combined, filtered, and evaporated to give compound 5 (1.35 g) as a brownish oil which was used in the next step without further purification.

³¹P{¹H} NMR (121.4 MHz, D₂O, pD = 3.9): 7.68 (1P, s). ³¹P NMR (121.4 MHz, D₂O, pD = 3.9): 7.68 (1P, t, ²J_{HP} = 12.5). MS-ESI: (+) 574.0 ([M + H]⁺, calcd 574.3); 611.9 ([M + K]⁺, calcd 612.2); 633.9 ([M + Na + K – H]⁺, calcd 634.2); (–) 571.8 ([M – H][–], calcd 572.3); 609.8 ([M + K – 2H][–], calcd 610.2).

Synthesis of H₅do3aNP. Crude product 5 (1.30 g) was dissolved in 20% aq CH₃CO₂H (50 mL). Next, Pd/C catalyst (10%, 0.26 g) was added, and the flask was evacuated and filled by H₂. The mixture was stirred under a hydrogen atmosphere (using a rubber balloon) for 48 h at room temperature (RT). Then, the catalyst was removed by filtration, and all volatiles were evaporated *in vacuo*. The product H₅do3aNP was purified by chromatography on a strong cation exchanger column (Dowex 50, H⁺-form, 3 cm × 15 cm). Impurities were removed by elution with water, and the product H₅do3aNP was eluted with 5% aq pyridine. The fractions containing the product were combined, filtered, and evaporated to dryness leaving a glassy solid which was dissolved in a small amount of water and crystallized by standing for 2 h. The white crystalline solid was isolated by filtration, washed with EtOH, and air-dried to give a white powder of hydrate H₅do3aNP·4.5H₂O (1050 mg, 44% based on tBu₃do3a·HBr).

¹H NMR (600 MHz, D₂O, pD = 5.81, Figure S5): δ 2.86–2.94 (4H, br m, macrocyclic CH₂); 3.00–3.05 (4H, br, NCH₂CH₂NH +

macrocyclic CH₂); 3.07–3.10 (2H, br m, macrocyclic CH₂); 3.20 (2H, br s, CH₂CO₂); 3.23 (2H, d, ²J_{HP} = 12.0, NCH₂P); 3.30 (2H, br t, ³J_{HH} = 5.0, NCH₂CH₂NH); 3.30–3.37 (2H, br m, macrocyclic CH₂); 3.42–3.45 (2H, br m, macrocyclic CH₂); 3.53–3.56 (2H, br m, macrocyclic CH₂); 3.69–3.72 (2H, br m, macrocyclic CH₂); 3.88 (4H, AB-multiplet, CH₂CO₂). ¹³C{¹H} NMR (150.9 MHz, D₂O, pD = 5.81, Figure S6): δ 45.78 (1C, d, ¹J_{CP} = 136, NCH₂P); 46.54 (1C, d, ³J_{CP} = 3.5, CH₂NHCH₂P); 48.97 (2C, macrocyclic CH₂); 49.00 (2C, macrocyclic CH₂); 50.36 (1C, CH₂CH₂NCH₂P); 51.08 (2C, macrocyclic CH₂); 53.02 (2C, macrocyclic CH₂); 55.71 (1C, CH₂CO); 57.83 (2C, CH₂CO); 170.92 (2C, CH₂CO); 178.98 (1C, CH₂CO). ³¹P{¹H} NMR (121.4 MHz, D₂O, pD = 5.81, Figure S7): δ 9.37 (1P, s). ³¹P NMR (121.4 MHz, D₂O, pD = 5.81, Figure S8): δ 9.37 (1P, t, ²J_{HP} = 12.0). MS-ESI: (+) 483.6 ([M + H]⁺, calcd 484.2); 505.6 ([M + Na]⁺, calcd 506.2); (–) 481.3 ([M – H][–], calcd 482.2); 519.1 ([M + Cl][–], calcd 518.2). Elemental analysis found (calcd for H₅do3aNP·4.5H₂O, C₁₇H₄₃N₅O_{13.5}P, M_r = 564.4): C, 36.22 (36.17); H, 8.09 (7.68); N, 12.17 (12.41); P, 5.61 (5.49).

Synthesis of Eu(III)–H₅do3aNP Complex. Three procedures for preparation of the Eu(III) complex of H₅do3aNP for NMR and MRI experiments were used. In the first one, EuCl₃·6H₂O was mixed with 1.05 equiv of the ligand in a small amount of distilled water. The pH was adjusted to 7 with 1 M aq NaOH, and the solution was stirred overnight at 60 °C. Then, the pH was readjusted to 7 with 1 M aq NaOH, and the solution was again stirred overnight at 60 °C.

In the second case, the Eu(III) complex was prepared by mixing the ligand with 1 equiv of Eu(III) acetate stock solution (concentration was determined by measuring BMS shifts)²⁸ in a small amount of distilled water. The pH was adjusted to ~8 with concentrated aq NH₃, and the mixture was stirred overnight at 60 °C. Then, the solution was filtered and evaporated to dryness leaving a glassy solid, which was dissolved in distilled water and evaporated on a rotary evaporator at 90 °C to remove ammonium acetate (this procedure was then repeated five more times).

In the third case, the Eu(III) complex was prepared by mixing EuCl₃·6H₂O with 1.05 equiv of the ligand in a small amount of distilled water. The pH was adjusted to ~8 with 0.8 M aq (NMe₄)OH, and the mixture was stirred overnight at 60 °C.

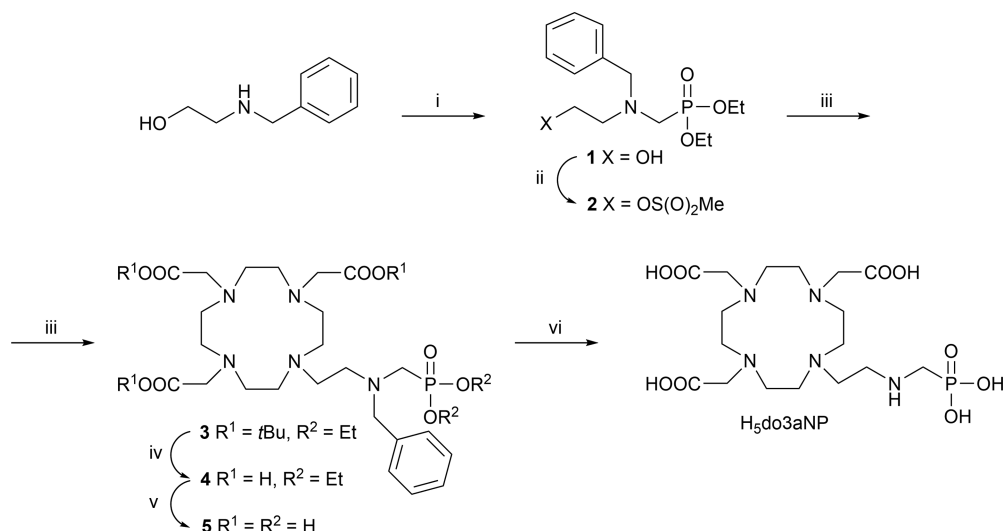
All prepared samples were checked using the xylenol orange test (acetate buffer, pH = 5.7) to exclude the presence of free Eu(III) ions. The exact concentration of Eu(III) complex in solution was determined using Evans' method.²⁸

Eu(III)–H₅do3aNP MS-ESI: (–) 631.6 with appropriate isotopic pattern ([M – H][–], calcd 632.1).

X-ray Diffraction Study. Single crystals of H₅do3aNP·4.75H₂O were prepared by slow evaporation of the aqueous solution of H₅do3aNP. Diffraction data were collected by employing an ApexII CCD diffractometer using Mo Kα radiation (λ = 0.71073 Å) at 150(1) K and analyzed using the SAINT V8.27B (Bruker AXS Inc., 2012) program package. The structures were solved by direct methods (SHELXS97)²⁹ and refined by full-matrix least-squares techniques (SHELXL97).³⁰ Relevant data for the structures have been deposited at the Cambridge Crystallographic Data Centre. The structure was solved in space group P1, where the independent unit consists of two ligand molecules which have very similar conformations. However, higher symmetry (*c*/2) is prevented by disorder of the phosphonate moiety of one of the units. The 10 highest isolated electronic maxima were attributed to the water solvate molecules, one of them half-occupied due to collision with one position of disordered phosphonate oxygen atoms. All non-hydrogen atoms were refined anisotropically, and hydrogen atoms were fixed in theoretical (C–H, N–H) or original (O–H) positions using a riding model U_H = 1.2U_X.

Crystal data follow: H₅do3aNP·4.75H₂O, C₁₇H_{43.5}N₅O_{13.75}P, M = 569.04, triclinic, *a* = 11.0215(3) Å, *b* = 12.3502(3) Å, *c* = 19.0688(6) Å, α = 84.311(1)°, β = 80.106(1)°, γ = 81.467(1)°, U = 2521.46(12) Å³, space group P1, *z* = 4, 11576 total reflections, 8615 intense reflections, R1[*I* > 2σ(*I*)] = 0.0535, wR2(all data) = 0.1543. CCDC-1500120.

Potentiometry. Potentiometric titrations were carried out in a thermostated (25.0 ± 0.1 °C) vessel at a constant ionic strength [*I* =

Scheme 1. Synthesis of H₅do3aNP^a

^a(i) HP(O)(OEt)₂, (CH₂O)_{*n*}, dry MeCN, 60 °C, 2 days; (ii) CH₃SO₂Cl, Et₃N, dry CH₂Cl₂, 0 °C–RT, 20 min; (iii) *t*Bu₃do3a-HBr, K₂CO₃, dry MeCN, RT, 24 h; (iv) CF₃COOH:CHCl₃ (1:1), reflux 18 h; (v) conc aq HCl, 95 °C, 24 h; (vi) H₂, Pd/C, 20% aq CH₃COOH, RT, 2 days.

0.1 M (Me₄N)Cl]. Measurements were taken with an excess of HCl stock solution added to the initial mixture, and the mixtures were titrated with stock solution of (NMe₄)OH. The ligand concentration in the titration vessel was ca. 0.004 M. An inert atmosphere was provided by a constant passage of argon saturated with water vapor. Before and after each titration, calibrations [titrations of HCl stock solution with (NMe₄)OH stock solution] were performed for determination of electrode calibration parameters as described previously.³¹

For determination of the ligand protonation constants, a standard technique was used,³¹ with the initial volume ca. 5 cm³ and in the pH range 1.9–12.1. Four titrations were carried out with ~70 points per titration.

Titrations of the Eu(III)–H₅do3aNP system were performed by an out-of-cell technique³¹ as the equilibrium was established slowly. In the experiments, the metal-to-ligand molar ratio was 1.00:1.04, and the starting volume of each titration point [before addition of (NMe₄)OH] was ca. 1 cm³. In total, two titration sets in the pH range 1.8–9.0 were prepared with 30 points per titration, and ampules with solutions were flame-sealed. After 4 weeks (waiting time for equilibration), the potential of each solution was determined with a freshly calibrated electrode, with measurement of odd and even data points separately affording four independent data series of 15 data points.

A preformed Eu(III) complex for determination of its protonation constants was prepared in the following way: in the ampule, equimolar amounts of the ligand and metal stock solutions were mixed, and a calculated amount (based on out-of-cell titration data) of (NMe₄)OH stock solution was gradually added to reach pH ca. 6, which corresponds to full complexation according to the out-of-cell titration. Ampules were flame-sealed and left at 55 °C for 3 days. From the final solution, aliquot volumes were pipetted, a defined amount of HCl stock solution was added into these samples, and the mixtures were immediately titrated by (NMe₄)OH stock solution in an analogous way as described above for the determination of the ligand protonation constants; the concentration of the complex in the titration vessel was ca. 0.003 M. The pH range used in these titrations was 1.9–9.5, and the titrations were carried out four times with 30 points per titration.

The OPIUM program package³² was used for calculation of the ligand protonation constants and stability/protonation constants of the Eu(III) complex. All constants are concentration constants. Calculated protonation constants are defined as $\beta_h = [H_hL]/\{[H]^h[L]\}$, and they can be transferred to consecutive protonation constants $\log K$ by $\log K(H_hL) = \log \beta_h - \log \beta_{h-1}$. Calculated stability constants β_{hlm} are defined by $\beta_{hlm} = [H_hL_hM_m]/\{[H]^h[L]^l[M]^m\}$.

Calculated constants with their standard deviations are compiled in Tables S8–S10, and the fits of titration data are shown in Figures S27, S31, and S32. The water ion product used in all calculations was $pK_w = 13.81$.³³

³¹P and ¹H NMR Titration of H₅do3aNP and Its Eu(III) Complex. ³¹P and ¹H NMR spectra were performed on a VNMR300 (B₀ = 7.05 T) using 5 mm sample tubes. A coaxial capillary with 85% H₃PO₄ in H₂O ($\delta_p = 0$) or with *t*BuOH in D₂O ($\delta_H = 1.25$) as the external standard was used. Solution pH was measured with a combined glass electrode (Spinrode Hamilton) employing a pH meter (3505 pH Meter, JENWAY) calibrated with standard buffers. Protonation constants were calculated with the OPIUM software package.³²

³¹P NMR titration (46 points) for determination of protonation constants and sites of H₅do3aNP was performed at 25 °C (0.05 M ligand concentration; no ionic strength control) in H₂O. The solution pH (0.1–13.6) was adjusted with aq HCl or aq (NMe₄)OH solutions. The fit is shown in Figure S28.

¹H NMR titration of H₅do3aNP in the alkaline region (14 points) was performed at 25 °C (0.05 M ligand concentration; no ionic strength control) in H₂O. Solution pH (7.9–12.0) was adjusted with aq HCl or aq KOH solutions. The fit is shown in Figure S29.

³¹P NMR titration in acidic region (14 points) of preformed Eu(III)–H₅do3aNP complex was performed at 25 °C (0.038 M complex concentration; ~150 mM NaCl) in H₂O. Solution pH (from 7.0 to 2.0) was adjusted with aq HCl solutions. The fit is shown in Figure S20.

MRS Experiments. A phantom consisting of one vial containing an aq solution of H₃PO₄ as a reference and three vials containing ~50 mM aq solutions of the Eu(III)–H₅do3aNP complex (~150 mM NaCl) with different pH values (6.4, 8.0, and 9.0) was prepared for MRS experiments. At these pH values, the once protonated complex [Eu(Hdo3aNP)][–] and the fully deprotonated species [Eu-(do3aNP)]^{2–} are present, with the former predominant at pH = 6.4 and the latter at pH = 9.0. At pH = 8.0, both species are present in similar abundance (see distribution diagram in Figure 6).

All MRS experiments were performed on a 4.7 T MR scanner BioSpec (Bruker BioSpin, Germany) using a dual ¹H/³¹P surface coil with a diameter of 5 cm (Bruker BioSpin, Germany). Nonlocalized ³¹P MRS spectra of the phantom were acquired by using a single rectangular pulse with 0.064 ms duration and 20000 Hz bandwidth (BW); the other measurement parameters were the following: acquisition delay 0.05 ms, repetition time (TR) = 1000 ms, number of acquisitions (NA) = 512, and scan time 8.5 min. For ¹H reference

images, a turbo spin echo sequence was used with the following parameters: TR/TE = 3000 ms/12 ms, turbo factor = 8, matrix size of 256×256 , field of view (FOV) = 35 mm \times 35 mm, slice thickness 1 mm, and scan time 5 min. ^{31}P MRSI spectra localized from 4×4 voxels covering the whole phantom volume were acquired by chemical shift imaging sequence using the same rectangular pulse as for the nonlocalized ^{31}P MR spectra. Spectral width 20 kHz (246.44 ppm) was sampled by 8192 points. The spectra were acquired by 16384 accumulations from the volume with field of view = 32 mm \times 32 mm and slice thickness 10 mm; the other parameters were TR = 1000 ms, effective echo time (TE_{eff}) = 15 ms, and scan time 4.5 h. Raw data were interpolated to a matrix $32 \times 32 \times 8192$ by zero-filling, and Fourier transform provided a three-dimensional matrix of numbers containing information about signal amplitude spatially encoded in x - and y -axis; frequency chemical shift was encoded in z -axis.

^{31}P MRSI data were processed using ImageJ software (version 1.46r, National Institutes of Health). First, the data were interpolated into a matrix size of $256 \times 256 \times 256$. Then, the images acquired within an interval of 70 ± 4 ppm were summed (to obtain an integral signal) as well as the images in the interval of 0 ± 4 ppm and -118 ± 4 ppm, and were finally false color coded.

RESULTS AND DISCUSSION

Synthesis. The target ligand $\text{H}_5\text{do3aNP}$ was prepared following the multistep synthesis outlined in Scheme 1. The key phosphorus-containing intermediate **1** was obtained by Mannich-type reaction of *N*-benzyl-ethanolamine with diethylphosphite and paraformaldehyde and was isolated after cation-exchange chromatography. It was converted to alkylation agent **2** by reaction with methanesulfonyl chloride, and compound **2** was used in the reaction with $t\text{Bu}_3\text{do3a}$, affording intermediate **3**. After sequential deprotection of *t*Bu-ester and ethyl-ester groups using trifluoroacetic acid and aq hydrochloric acid, respectively, the de-esterified compound **5** was hydrogenated using the Pd/C catalyst to give the target ligand $\text{H}_5\text{do3aNP}$ that was purified by cation-exchange chromatography and was isolated in the zwitterionic form in the overall 44% yield (based on $t\text{Bu}_3\text{do3a}\cdot\text{HBr}$).

The target ligand $\text{H}_5\text{do3aNP}$ was structurally characterized by single-crystal X-ray diffraction analysis. In the crystal structure of $\text{H}_5\text{do3aNP}\cdot 4.75\text{H}_2\text{O}$, two independent ligand molecules are present, but both adopt a very similar conformation. Therefore, only one of them is shown in Figure 2. A zwitterionic molecule is protonated on two nitrogen atoms of the macrocycle (those bearing the “*trans*” acetate groups) and the nitrogen atom of the side arm. The remaining protons are located on the phosphonate and on the “odd” acetate groups. Molecular conformation is stabilized by medium-strength intramolecular hydrogen bonds (Table S1), and the whole structure is stabilized through a wide system of intermolecular hydrogen bonds involving water molecules.

Solution Structure of the Eu(III)– $\text{H}_5\text{do3aNP}$ Complex. Ln(III) complexes of the DOTA-like ligands are typically present in a solution as a mixture of square-antiprismatic (SA) and twisted-square-antiprismatic (TSA) isomers.³⁴ These isomers differ in conformation of the five-membered chelate rings of the macrocycle (δ/λ) and course of rotation of the pendant arms (Δ/Λ). Combination of the macrocycle and pendant conformations results in two diastereomeric pairs of the enantiomers (Figure S9). The pair $\Delta\lambda\lambda\lambda\lambda/\Lambda\delta\delta\delta\delta$ forms the SA arrangement while the $\Delta\delta\delta\delta\delta/\Lambda\lambda\lambda\lambda\lambda$ enantiomers correspond to the TSA structure.³⁵ Typically, two diastereomers are in a slow exchange with respect to the time scale of an NMR experiment, giving rise to two sets of ^1H NMR signals. Therefore, both isomers can be distinguished, and their relative

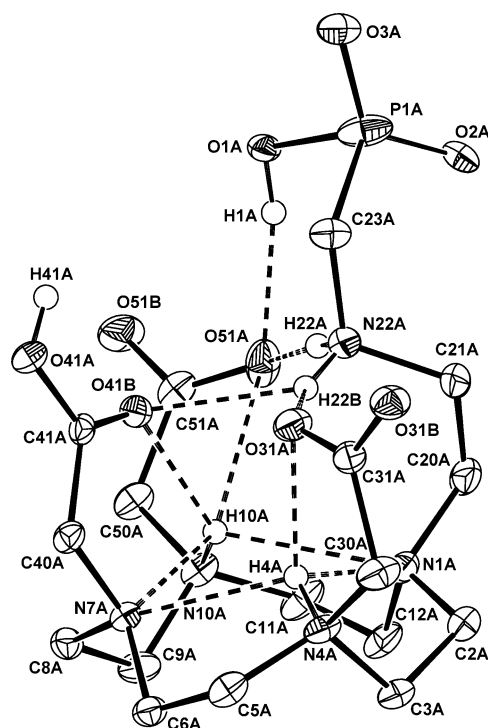


Figure 2. Molecular structure of $\text{H}_5\text{do3aNP}$ found in the crystal structure of $\text{H}_5\text{do3aNP}\cdot 4.75\text{H}_2\text{O}$. Intramolecular hydrogen bonds are dashed (Table S1).

abundance in solution can be easily determined. Isomerism evaluation mostly uses signals of “axial” protons of the macrocyclic ring (Figure S9) because these are the closest ones to the Ln(III) ion and to the principal magnetic axis; thus, they are shifted away from the other signals in the ^1H NMR spectra. Typically, “axial” signals of the TSA species of Eu(III) complexes with DOTA-like ligands are found in the ~ 7 – 28 ppm range whereas those of the SA isomers appear in the ~ 25 – 40 ppm region.³⁶

Solution structure of the Eu(III) complex species was investigated by ^1H NMR spectroscopy in the pD range 6.8–9.9 (Figure 3 and Figure S10). At pD < 7.3, only one set of signals was observed in the ^1H NMR spectra, where the signals of the most positively shifted “axial” protons of the complex species appear in the range typical for the SA isomer (20–49 ppm). At higher temperatures, the ^1H NMR signals somewhat shift and broaden due to faster conformational changes of the complex molecule (Figure S11). With increasing pD, ^1H NMR signals of the SA isomer gradually disappear with a simultaneous appearance of peaks attributable to the TSA isomer with the most shifted signals in the 7–14 ppm range (Figure 3 and Figure S10). Thus, one can suggest that both SA and TSA species are present in the pD range 7.5–9.0 (Figures S10, S12, and S13). At pD > 9.0, only signals of pure TSA species were detected. Heating of the alkaline solution also led to a significant broadening of signals of the TSA isomer, pointing to conformational change of the complex molecule (Figures S12 and S14). On the basis of these observations, one can suggest that two differently protonated species are present in the pD range 7.5–9.0; so, the pK_a of the deprotonation process lies in this range, and thus, the deprotonation obviously occurs on the pendant amino group. The protonated form of the complex exists exclusively in the SA isomer, whereas the pure TSA species is formed upon deprotonation.

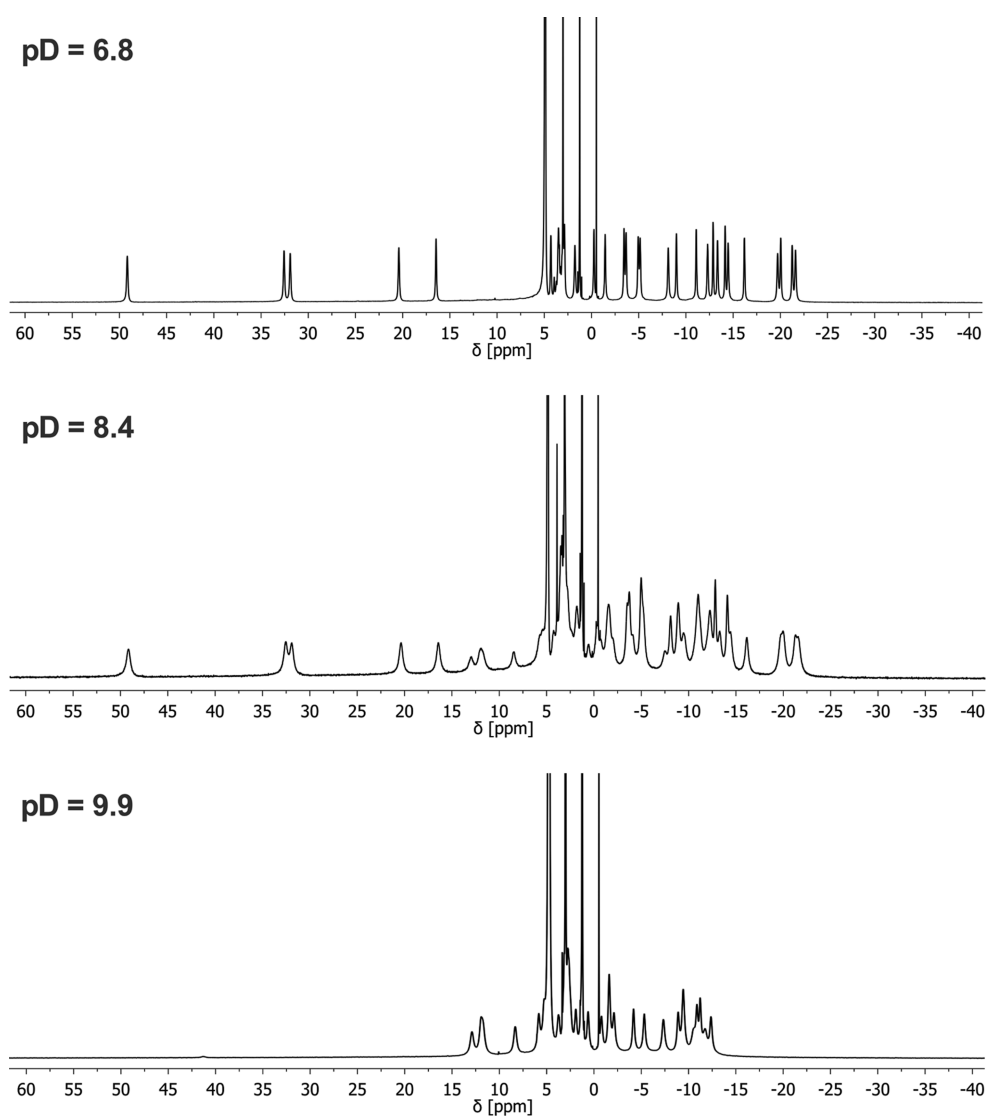


Figure 3. ^1H NMR spectra of $\text{SA}[\text{Eu}(\text{Hdo3aNP})]^-/\text{TSA}[\text{Eu}(\text{do3aNP})]^{2-}$ (~ 0.08 M solution in D_2O , $B_0 = 7.05$ T) at different pD values.

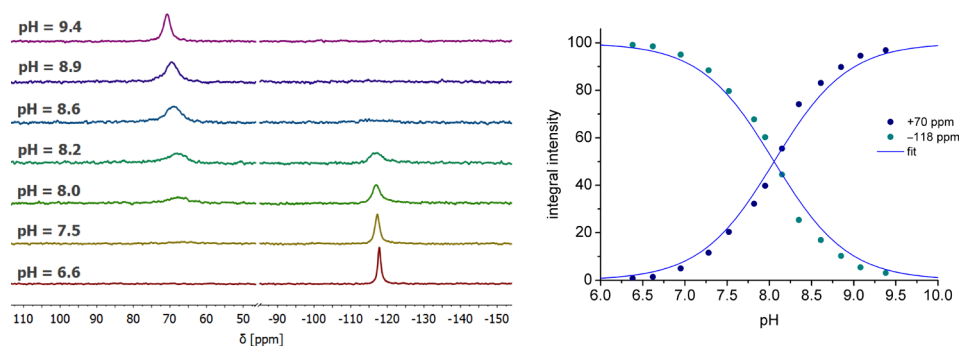


Figure 4. $^{31}\text{P}\{^1\text{H}\}$ NMR spectra of $\text{SA}[\text{Eu}(\text{Hdo3aNP})]^-/\text{TSA}[\text{Eu}(\text{do3aNP})]^{2-}$ complex species at various pH values and corresponding pH dependence of an integral intensity of ^{31}P NMR signals (50 mM solution in H_2O , ~ 150 mM NaCl, $B_0 = 7.05$ T, 25°C).

^{31}P NMR spectroscopic study also revealed a slow chemical exchange between both complex species with respect to the time scale of the NMR experiment (Figure 4 and Figures S16 and S18) as the signals of both species are present in the ^{31}P NMR spectra acquired in the pH range 7.5–8.9; their chemical shifts remain nearly constant with pH change. ^{31}P NMR 1D-EXSY revealed a rate for isomer interconversions on a

millisecond scale (rate constants $191(8) \text{ s}^{-1}$ for $\text{SA} \rightarrow \text{TSA}$ and $156(7) \text{ s}^{-1}$ for $\text{TSA} \rightarrow \text{SA}$ rearrangements, respectively, 25°C , pD = 8.6). In addition, an extreme chemical shift difference (by ~ 190 ppm) between signals of the SA and TSA species was observed. In both species, the phosphonate group is obviously coordinated, as evidenced by a significantly influenced ^{31}P NMR chemical shift (+70 ppm for the TSA and -118 ppm for

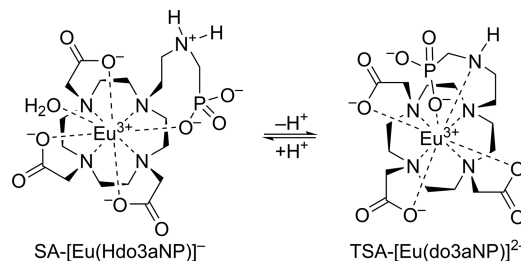
the SA species, respectively, Figure 4) compared to that for the diamagnetic La(III) complex ($\delta = 25.3$ ppm at $pD = 7.0$ and $\delta = 22.7$ ppm at $pD = 10.1$). The coordination of the phosphonate group was also confirmed by measurement of T_1 relaxation times of ^{31}P NMR signal, which are $T_1 = 0.207(4)$ s for the SA species (measured at $pD = 6.8$) and $T_1 = 0.202(11)$ s for the TSA species ($pD = 9.6$), respectively, whereas the La(III) complex relaxes much slower with $T_1 = 1.84(8)$ s ($pD = 7.0$) and $T_1 = 3.09(10)$ s ($pD = 10.1$).

The dependence of integral intensities of these signals on pH is sigmoidal and, in accordance with the suggestion stated above, could be successfully modeled by an equilibrium involving just one (de)protonation step (Figure 4 and Figures S16–S18), affording the protonation constant $\log K(=pK_A) = 7.4\text{--}8.5$ with dependence on ionic strength, see Table S2. The ^{31}P chemical shifts of both species (Figures S16 and S18) and derived protonation constants (Table S2) are independent of complex concentration; therefore, intermolecular coordination of the phosphonate to the metal ion belonging to a different complex molecule and the formation of polynuclear complexes can be excluded. Furthermore, the protonated complex was found to be fully stable at $pD = 5.9$ (Figure S19). The value of the protonation constant $\log K$ is dependent on the quality and concentration of a background electrolyte: in the presence of NaCl, the value drops with increasing concentration of the salt because the presence of a coordinating metal ion generally facilitates a deprotonation of the donor atoms. In contrast, when $(\text{NMe}_4)\text{Cl}$ as the background electrolyte, the value of the protonation constant was significantly higher (Table S2). In the presence of CaCl_2 and MgCl_2 , i.e., in the presence of stronger coordinating metal ions (Figure S18), the chemical shifts in ^{31}P NMR spectra remain unaffected, and $\log K$'s are lower than those calculated in the case of NaCl-containing solutions (Table S2).

On the basis of the value of $\log K$, the protonation process obviously occurs on the pendant arm amino group, and thus, one can conclude that the equilibrium involves monodeprotonated and fully deprotonated complex species; thus, the complex species are $\text{SA-}[\text{Eu}(\text{Hdo3aNP})]^-$ and $\text{TSA-}[\text{Eu}(\text{do3aNP})]^{2-}$. To confirm such an assignment, the ^1H NMR spectra were also measured in H_2O solution. In a slightly acid region, no difference between the spectra of $\text{SA-}[\text{Eu}(\text{Hdo3aNP})]^-$ acquired in D_2O and H_2O was found (Figure S15A,B). At this pH, the side amino group is protonated (and thus uncoordinated), and the hydrogen atoms are exchanged with the solvent (D_2O) or overlaid with others; on the basis of chemical exchange saturation transfer experiments, chemical shift of these hydrogen atoms is -17 ppm if referenced as $\delta(\text{H}_2\text{O}) = 0$.³⁷ In contrast, in a slightly alkaline region, a new signal at 36.4 ppm (if referenced as $\delta(\text{H}_2\text{O}) = 0$) appeared in the spectra of $\text{TSA-}[\text{Eu}(\text{do3aNP})]^{2-}$ acquired in H_2O (Figure S15C,D). This peak can be attributed to a hydrogen atom bound in the coordinated pendant secondary amino group, where this hydrogen atom is not in fast exchange with the solvent. This assignment is also supported by a similarity in the chemical shift of this signal to the values observed for structurally related compounds $[\text{Eu}(\text{do3a-ae})]$ and $[\text{Eu}(\text{do3aNN})]$ (Figure 1), respectively; one of the ^1H NMR signals of the coordinated primary amino group in $[\text{Eu}(\text{do3a-ae})]$ lies at 34 ppm,⁴⁴ and the signal of one of the isomers of $[\text{Eu}(\text{do3aNN})]$ with a coordinated secondary amino group is located at 35 ppm.¹⁵

With mononuclearity of the complex species taken into account, electrostatic repulsion of the central metal ion and the protonated pendant amino group, as well as general steric hindrances, the phosphonate group should be in the protonated $\text{SA-}[\text{Eu}(\text{Hdo3aNP})]^-$ species coordinated in the O_4 -plane (Scheme 2). In such a case, it opens a space for coordination of

Scheme 2. Suggested Geometry of the $\text{SA-}[\text{Eu}(\text{Hdo3aNP})]^-$ and $\text{TSA-}[\text{Eu}(\text{do3aNP})]^{2-}$ Species^a



^aA water molecule in the protonated species is expected to be coordinated in the apical position.

a water molecule in an O_4 -capping apical position. Luminescence lifetimes of Eu(III) ion were measured, giving $\tau = 697$ μs for $\text{SA-}[\text{Eu}(\text{Hdo3aNP})]^-$ species in H_2O ($\text{pH} = 6.4$) and $\tau = 2.21$ ms when this sample was evaporated and dissolved in D_2O , consistent with the assumption of water coordination.³⁸ After deprotonation, coordination of the secondary amino group occurs and forms an O_3N -coordination plane in the $\text{TSA-}[\text{Eu}(\text{do3aNP})]^{2-}$ species. The phosphonate group very probably moves to the position capping this O_3N -plane (Scheme 2). However, although the geometry discussed above is the sole possibility making chemical sense, it is a bit contradictory in a comparison of the ^{31}P NMR shift of $\text{SA-}[\text{Eu}(\text{Hdo3aNP})]^-$ species with that of Eu(III) complexes of DOTA-like ligands having methylenephosphonate/phosphinate pendant moieties, which have a phosphorus atom in a similar spatial position as that expected for $\text{SA-}[\text{Eu}(\text{Hdo3aNP})]^-$. To the best of our knowledge, in all Eu(III) complexes of phosphinate/phosphonate ligands reported previously, the paramagnetic contribution to the ^{31}P NMR shift is positive, giving signals with 15–70 ppm higher chemical shift compared to that of the free ligands or diamagnetic La(III) complexes (Table S3).^{36b,c,e,f,39,40} Contrary to these values, when comparing ^{31}P NMR shift differences between Eu(III) and La(III) complexes of $\text{H}_5\text{do3aNP}$ in acid media, the paramagnetic contribution to chemical shift of $\text{SA-}[\text{Eu}(\text{Hdo3aNP})]^-$ is $\Delta\delta = -143$ ppm.

The origin of this contradiction probably lies in the low symmetry of the ligand field of the $\text{SA-}[\text{Eu}(\text{Hdo3aNP})]^-$ complex, which can lead to a discrepancy between principal magnetic and pseudo- C_4 axes and to significant anisotropy of magnetically induced shifts.⁴¹ Typically, the complexes of DOTA-like ligands have (pseudo)- C_4 symmetry, and it is usually suggested that the principal magnetic axis is identical with (or very close to) the (pseudo)symmetry C_4 axis. In such axially symmetric systems, the phosphorus atoms lie outside the McConnell cone, which defines a sign of paramagnetic contribution to the chemical shift [in relevant crystal structures, angle between (pseudo)- C_4 axis and Ln–P vector is $73\text{--}89^\circ$ (Figure S22 and Table S4),^{36e,b,40,42} whereas the McConnell critical angle is 54.7°]. It should be noted that, for historical reasons, the direction of upfield–downfield shifts differs for ^1H

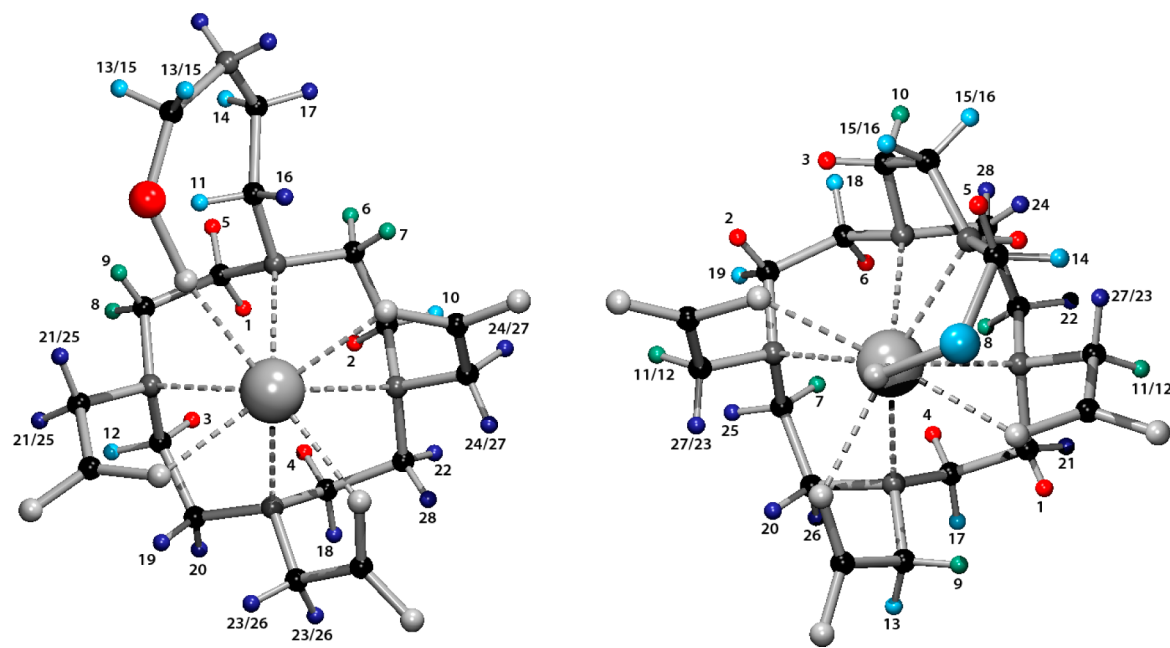


Figure 5. Assignment of the ^1H NMR spectra of $\text{SA}[\text{Eu}(\text{Hdo3aNP})]^-/\text{TSA}[\text{Eu}(\text{do3aNP})]^{2-}$ complex species. Geometry of the complex species is tentative and was not optimized. Atoms are labeled by order numbers from the spectra going from left to right according to Figure S24. For better visualization, protons with positive paramagnetic contribution are red, those with small negative contribution are pale blue, those with large negative contribution dark blue, and those which are not influenced are green. For phosphorus atom, the red color indicates a negative ^{31}P NMR shift contribution (i.e., position in space with positive ^1H NMR shift contribution), and blue indicates a positive ^{31}P NMR shift contribution (i.e., space with negative ^1H NMR shift contribution).

Table 1. Equilibrium Constants ($\log K$ and $\log K_{\text{ML}}$)^a of $\text{H}_3\text{do3aNP}$ (0.1 M NMe_4Cl , 25 °C) and Its Eu(III) Complexes and Comparison with Corresponding Constants Reported for Related Ligands

equilibrium	$\text{H}_3\text{do3aNP}$ potentiometry	$\text{H}_3\text{do3aNP}$ ^{31}P NMR	$\text{H}_3\text{do3aNN}^b$	$\text{H}_3\text{do3a-ae}^c$	H_4dota
$\text{H}^+ + \text{L}^{n-} \leftrightarrow \text{HL}^{1-n}$	12.56(1)	12.52(17)	12.62	13.19	12.9 ^e
$\text{H}^+ + \text{HL}^{1-n} \leftrightarrow \text{H}_2\text{L}^{2-n}$	10.37(1)	10.59(3)	10.28	10.51	9.72 ^e
$\text{H}^+ + \text{H}_2\text{L}^{2-n} \leftrightarrow \text{H}_3\text{L}^{3-n}$	9.23(1)	9.37(8)	9.67	8.90	4.60 ^e
$\text{H}^+ + \text{H}_3\text{L}^{3-n} \leftrightarrow \text{H}_4\text{L}^{4-n}$	6.17(1)	5.96(8)	8.30	3.87	4.15 ^e
$\text{H}^+ + \text{H}_4\text{L}^{4-n} \leftrightarrow \text{H}_5\text{L}^{5-n}$	4.19(1)		3.30	1.27	2.29 ^e
$\text{H}^+ + \text{H}_5\text{L}^{5-n} \leftrightarrow \text{H}_6\text{L}^{6-n}$	1.90(1)	2.05(9)	1.58		1.34 ^e
$\text{Eu}^{3+} + \text{L}^{n-} \leftrightarrow [\text{Eu}(\text{L})]^{3-n}$	23.49(3)		23.16	22.23 ^d	24.2 ^f
$\text{H}^+ + [\text{Eu}(\text{L})]^{3-n} \leftrightarrow [\text{Eu}(\text{HL})]^{4-n}$	8.00(3)		6.03	5.83 ^d	
$\text{H}^+ + [\text{Eu}(\text{HL})]^{4-n} \leftrightarrow [\text{Eu}(\text{H}_2\text{L})]^{5-n}$	3.75(4)		5.09		
$\text{H}^+ + [\text{Eu}(\text{H}_2\text{L})]^{5-n} \leftrightarrow [\text{Eu}(\text{H}_3\text{L})]^{6-n}$	4.35(4)				
$\text{H}^+ + [\text{Eu}(\text{H}_3\text{L})]^{6-n} \leftrightarrow [\text{Eu}(\text{H}_4\text{L})]^{7-n}$	3.31(4)				

^a $K = [\text{H}_n\text{L}]/\{[\text{H}][\text{H}_{n-1}\text{L}]\}$ or $[\text{H}_n\text{LM}]/\{[\text{H}][\text{H}_{n-1}\text{LM}]\}$; $K_{\text{ML}} = [\text{ML}]/\{[\text{L}]\cdot[\text{M}]\}$. ^bRef 15. ^cRef 44. ^dData reported for Gd(III) complex. ^eRef 45. ^fRef 33.

and ^{31}P NMR scales; therefore, in the same space, the ^{31}P NMR paramagnetic induced shift contribution is positive whereas that of ^1H NMR is negative (and *vice versa*). However, in the case of the $\text{SA}[\text{Eu}(\text{Hdo3aNP})]^-$ complex, there is a large difference in chemical shifts of “axial” macrocycle protons [these protons have a similar position with respect to pseudo- C_4 symmetry defined by the central ion and the barycenter of the N_4 -plane, and thus, they should have a similar chemical shift when the magnetic axis is identical to the (pseudo)symmetry axis]; this points to some difference between positions of pseudosymmetric- C_4 and principal magnetic axes. Therefore, the phosphorus atom could fall into a space close to the principal magnetic axis direction with induced positive ^1H /negative ^{31}P NMR shifts. To confirm this assumption, the signals found in ^1H NMR spectra of both $\text{SA}[\text{Eu}(\text{Hdo3aNP})]^-$ and $\text{TSA}[\text{Eu}(\text{do3aNP})]^{2-}$ complexes were assigned on the basis of ^1H

COSY and ^1H EXSY experiments and ^{13}C NMR spectra with selectively tuned ^1H decoupling (Figure S23–S26 and Tables S5–S7). The assignment is shown in Figure 5 (for detailed description see SI). This assignment confirmed that the position of the phosphorus atom moves from a space with induced positive ^1H /negative ^{31}P NMR shifts in $\text{SA}[\text{Eu}(\text{Hdo3aNP})]^-$ to an area with negative ^1H /positive ^{31}P NMR shifts in $\text{TSA}[\text{Eu}(\text{do3aNP})]^{2-}$ complexes, respectively. Another surprising finding is the fact that the most shifted signals in ^1H NMR spectra of $\text{TSA}[\text{Eu}(\text{do3aNP})]^{2-}$ species are not the “axial” ones. In this case, the direction of the most positive ^1H induced shift probably lies almost parallel in respect to the N_4 -plane, so the principal magnetic axis should be almost perpendicular to the pseudo- C_4 axis. The phosphorus atom falls outside this direction, and so, its induced ^{31}P paramagnetic shift is positive in the ^{31}P NMR scale.

Further acidification of the solution of the SA-[Eu(Hdo3aNP)]⁻ species leads to a gradual change of the ³¹P chemical shift from -118 ppm at pH = 7 to -156 ppm at pH = 2 (Figure S20). Obviously, as the chemical shift is very affected in the whole of this pH region, the phosphonate group is still coordinated, and the gradual change of the chemical shift corresponds to formation of the SA-[Eu(H₂do3aNP)] species. From the ³¹P NMR data, log *K* = 3.40(1) was calculated which confirms this assignment because the protonation constant of the free phosphonate group (log *K* ~ 5–7) drops to the log *K* ~ 3–4 range upon coordination to the metal ion.⁴³ Formation of the SA-[Eu(H₂do3aNP)] species was also supported by the ¹H NMR spectra of the complex in acidic solution (Figure S21).

Thermodynamic Behavior of H₃do3aNP and Its Eu(III) Complex. To obtain information on thermodynamic stability of the studied Eu(III) complex and confirm the conclusions stated above, potentiometric studies of the H₃do3aNP, equilibrated Eu(III)–H₃do3aNP system and preformed Eu(III)–H₃do3aNP complex were performed.

The potentiometric titrations of H₃do3aNP performed in the pH range 1.9–12.1 revealed six consecutive protonation processes (Table 1 and Table S8; fit shown in Figure S27); the ligand distribution diagram is shown in Figure S30. Five of these constants could also be calculated from the pH dependence of the ³¹P NMR spectra (Table 1 and Table S8, fit shown in Figure S28). On the basis of comparison with the literature data,⁴³ the first protonation step (log *K*(HL) = 12.56) can be attributed to a proton shared by the macrocycle amino groups. This assignment of the protonation site is consistent with a relatively small change (+0.5 ppm) of the ³¹P NMR shift and a large change of the ¹H chemical shift of the α -acetate protons (+0.21 and +0.28 ppm for “double” and “odd” acetates, respectively) compared to that of the NCH₂P group (+0.05 ppm), see Table S8 and Figure S29. According to the highest change (~6 ppm) in ³¹P chemical shift during the NMR titration, the second protonation step (log *K*(H₂L) = 10.37) obviously occurs on the amino group belonging to the pendant moiety. It is also consistent with changes observed in ¹H NMR spectra; change of δ (¹H) of NCH₂P is 0.25 ppm, much higher than the δ (¹H) changes of the acetate groups (0.11 and 0.08 ppm, respectively, see Table S8). The value of the protonation constant is higher than the value reported for the analogous protonation of the 2-aminoethyl arm for H₃do3a-ae (log *K* = 8.90)⁴⁴ due to the positive induction effect of the phosphonate moiety.⁴³ Analogous protonation of H₃do3aNN occurs in this pH region, although in that case it was not possible to assign an exact value due to a number of protonation steps occurring with similar log *K*'s.¹⁵ The third protonation (log *K*(H₃L) = 9.23) corresponds to the second protonation of the macrocycle amino groups. The log *K*(H₃L) is somewhat lower than the second ring-amine protonation of related ligands due to electrostatic repulsion with a protonated pendant amino group. The third protonation locks two protons on the macrocycle nitrogen atoms bearing “trans” acetate groups due to mutual electrostatic repulsion, as evidenced by change of δ (¹H) (+0.38 and -0.26 ppm for “double” and “odd” acetates, respectively, see Figure S29). The fourth protonation with log *K*(H₄L) = 6.17 occurs on the phosphonate moiety, as evidenced by a reverse change of the ³¹P NMR shift (Figure S28). The next one (log *K*(H₅L) = 4.19) is associated with the protonation of the acetate *trans* to the aminophosphonate arm, and it has no influence on the chemical shift of the ³¹P NMR

signal due to a long distance between these groups, so this constant cannot be calculated from ³¹P NMR data. The last (sixth) protonation occurs on one of the remaining acetate arms or macrocycle amino groups. The suggested protonation scheme is fully consistent with the molecular structure found in the solid state (see above).

The stability constant of the [Eu(do3aNP)]²⁻ complex (log *K*_{ML} = 23.49, Table 1) was obtained by an out-of-cell titration technique. The value falls into the expected range, as can be seen from a comparison with the stability constants reported for the related ligands (Table 1). According to the distribution diagrams of the Eu(III)–H₃do3aNP system shown in Figure 6, the metal ion complexation is quantitative at pH ~ 4.5.

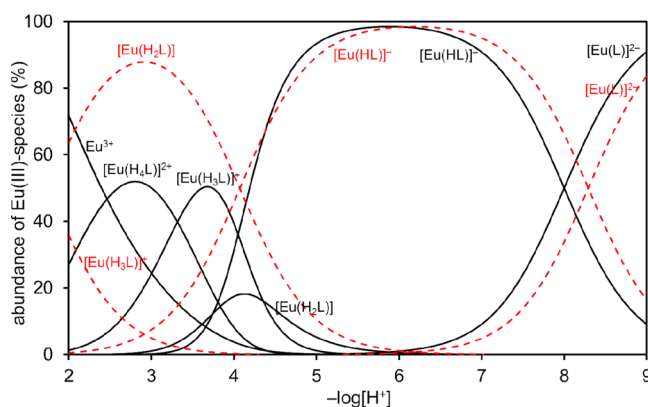


Figure 6. Distribution diagram of metal-containing species in the Eu(III)–H₃do3aNP system (black solid lines, *c*_M = *c*_L = 0.004 M) and of species present in acid–base titration of the preformed [Eu(do3aNP)]²⁻ complex (red dashed lines) Conditions: 25 °C, *I* = 0.1 M NMe₄Cl.

The first protonation of the fully deprotonated species, [Eu(do3aNP)]²⁻, proceeds with log *K*(HLM) = 8.0. In the analysis of the NMR spectra (see above), this protonation was suggested to occur on the side arm secondary amino group. The protonation constant of this group in the free ligand has the value log *K*(H₂L) = 10.37, and so a significant metal-induced decrease of this value confirms coordination of the deprotonated amino group to the central Eu(III) ion.

A further three protonation steps in the equilibrated solutions occur with log *K*'s in a narrow range ~3–4 (Table 1). These processes occur at pH higher than that corresponding to protonation of the coordinated acetate group and, thus, can be attributed to simultaneous protonations of the phosphonate group and the macrocycle nitrogen atoms. Therefore, the equilibrated species H₃LM and H₄LM are expected to be out-of-cage complexes with double-protonated macrocycle amino groups similar to those suggested for other systems with DOTA-like ligands.⁴⁰

To support the conclusions stated above, an acid–base titration of the preformed complex was performed. In this case, only three stepwise protonation constants were found: log *K*(HLM) = 8.29(2), log *K*(H₂LM) = 4.07(3), and log *K*(H₃LM) = 1.75(3) (see Table S10 and distribution diagram in Figure 6). According to the interpretation above, the first constant corresponds to a protonation of the pendant amino group, and this value is consistent with the results of ³¹P NMR and out-of-cell potentiometric studies. The second constant is assigned to protonation of the coordinated phosphonate group, consistent with the ³¹P NMR data presented above. The

differences between values obtained by the ^{31}P NMR and potentiometric titrations can be attributed to a difference in ionic strength, different methods of pH electrode calibration, and temperature of the pH measurement. The third constant calculated for the preformed complex is significantly lower compared to constants observed in the equilibrated solutions (out-of-cell titration). One can assume that during the short time scale of the potentiometric titration only the in-cage complex is present (i.e., no dissociation of macrocycle–Eu(III) bonds occurs) due to relative kinetic inertness of the complexes with DOTA-like ligands,¹ and therefore, this constant corresponds very probably to the protonation of a coordinated carboxylate group.

Overall, the results of the potentiometric study are fully consistent with the results of ^{31}P NMR studies discussed above and support the interpretation shown in Scheme 2.

pH Mapping Using MRS. To address possible pH determination from ^{31}P NMR data, the logarithm-weighted ratio of integral intensity of the ^{31}P NMR signals of TSA- $[\text{Eu}(\text{do3aNP})]^{2-}$ and SA- $[\text{Eu}(\text{Hdo3aNP})]^{-}$ was calculated. This function is linear in the pH range 6.5–9.5, as shown in Figure 7, proving the principle of the suggested method (the data were observed at various experimental conditions).

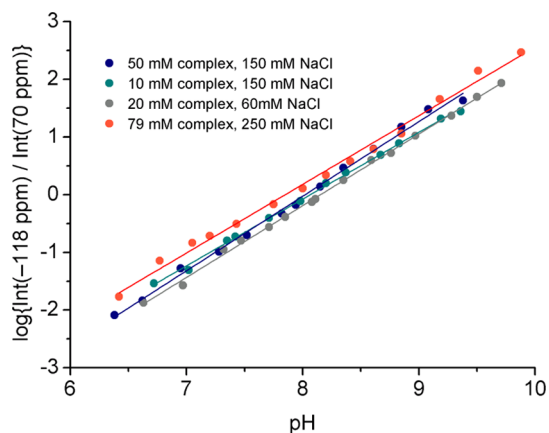


Figure 7. Dependence of $y = \log\{\text{Int}(-118 \text{ ppm})/\text{Int}(70 \text{ ppm})\} \sim \log\{[\text{SA}]/[\text{TSA}]\}$ on pH in solutions with different concentrations of the complex probe and at different ionic strengths relevant for physiologic conditions.

Finally, we tested the applicability of the $[\text{Eu}(\text{do3aNP})]^{2-}/[\text{Eu}(\text{Hdo3aNP})]^{-}$ system as a pH probe for MRI. However, this experiment had some limitations due to the accessible hardware. The broad spectral width (20 kHz/246 ppm) necessary for the experiment required a short excitation pulse. Due to hardware limitations, a block pulse (instead of modulated one) had to be used for excitation to reach sufficient pulse intensity. As the excitation profile of the block pulse is inhomogeneous, intensities at different frequencies may not exactly correspond to the concentrations. The space-localized ^{31}P MR spectra were measured in the phantom consisting of four vials: a vial containing an aqueous solution of H_3PO_4 as a reference and three vials containing the Eu(III)– $\text{H}_5\text{do3aNP}$ complex solutions having different pH values (6.4, 8.0, and 9.0). The localized spectra and intensity of individual signals from different parts of the phantom are shown in Figure 8, and the results clearly show a spatial resolution of areas with different pH values, proving the suggested concept.

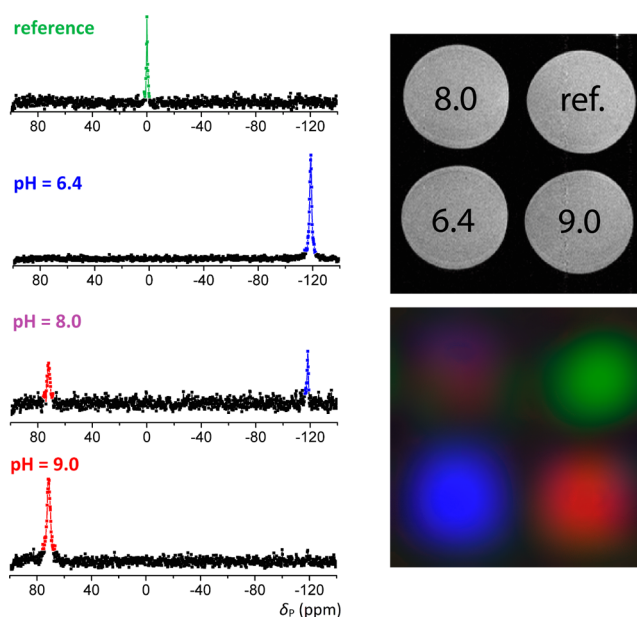


Figure 8. Left: localized ^{31}P MR spectra. Right: pH map and legend (^1H MR reference image) of phantom consisting of one vial containing aqueous H_3PO_4 as a reference and three vials containing aqueous solutions of the Eu(III)– $\text{H}_5\text{do3aNP}$ complex with different pH values. Postprocessing included interpolation to a spatial 256×256 matrix, integration over the selected signals, and false color coding. Color scheme: red, signal at +70 ppm; blue, –118 ppm; purple color results from red/blue superposition; green, 0 ppm.

CONCLUSIONS

New ligand $\text{H}_5\text{do3aNP}$ with a 2-[amino(methylphosphonic acid)]ethyl pendant arm was synthesized, and its coordination properties were studied by potentiometry and NMR spectroscopy. Full in-cage complexation of Eu(III) is finished at $\text{pH} > 4.5$, forming the protonated SA- $[\text{Eu}(\text{Hdo3aNP})]^{-}$ complex with square-antiprismatic (SA) geometry. Upon deprotonation with $\text{p}K_A \sim 8$, the twisted-square-antiprismatic TSA- $[\text{Eu}(\text{do3aNP})]^{2-}$ complex is formed. Both complexes are in a slow equilibrium on the NMR time scale, and their ^{31}P NMR shifts differ by ~ 190 ppm due to significant movement of the principal magnetic axis leading to different paramagnetic contributions to the ^{31}P NMR shift. To the best of our knowledge, such a strict change of the coordination geometry with (de)protonation has not been observed before.

The existence of two separate signals in the ^{31}P NMR spectra allows ratiometric determination of pH by MRS. As both signals belong to the same compound (differing just by its protonation state), this ensures the same biodistribution of both species, and the ratiometric approach brings the advantage of independence of the measured data on the probe concentration. Unfortunately, the $\text{p}K_A$ of the studied complex lies somewhat outside the region optimal for *in vivo* use; nevertheless, this parameter can be altered by a suitably designed ligand, and thus, the discovered principle shows promising potential for *in vivo* applications.

ASSOCIATED CONTENT

Supporting Information

The Supporting Information is available free of charge on the ACS Publications website at DOI: 10.1021/acs.inorgchem.6b02749.

NMR spectra and studies, hydrogen bond lengths, and potentiometric results (PDF)
Crystal data (CIF)

AUTHOR INFORMATION

Corresponding Author

*E-mail: modrej@natur.cuni.cz. Phone: +420-221951261. Fax: +420-221951253.

ORCID

Jan Kotek: 0000-0003-1777-729X

Notes

The authors declare no competing financial interest.

ACKNOWLEDGMENTS

We thank Z. Böhmová for the potentiometric measurements and Dr. I. Císařová for the X-ray diffraction study. Support from the Grant Agency of the Czech Republic (Project 16-03156S) is acknowledged. We really appreciate remarks from the referees regarding the spatial dependence of the paramagnetic contribution to chemical shift.

REFERENCES

- (1) *The Chemistry of Contrast Agents in Medical Magnetic Resonance Imaging*, 2nd ed.; Merbach, A., Helm, L., Tóth, E., Eds.; Wiley: Chichester, United Kingdom, 2013.
- (2) Gillies, J. R.; Raghunand, N.; Garcia-Martin, M. L.; Gatenby, R. A. pH imaging: A review of pH measurement methods and applications in cancers. *IEEE Eng. Med. Biol.* **2004**, *23*, 57–64.
- (3) Hingorani, D. V.; Bernstein, A. S.; Pagel, M. D. A review of responsive MRI contrast agents: 2005–2014. *Contrast Media Mol. Imaging* **2015**, *10*, 245–265.
- (4) Zhu, L.; Yang, Y.; Farquhar, K.; Wang, J.; Tian, C.; Ranville, J.; Boyes, S. G. Surface Modification of Gd Nanoparticles with pH-Responsive Block Copolymers for Use As Smart MRI Contrast Agents. *ACS Appl. Mater. Interfaces* **2016**, *8*, 5040–5050.
- (5) (a) Zhang, S.; Wu, K.; Sherry, A. D. A Novel pH-Sensitive MRI Contrast Agent. *Angew. Chem., Int. Ed.* **1999**, *38*, 3192–3194. (b) Raghunand, N.; Howison, C.; Sherry, A. D.; Zhang, S.; Gillies, R. J. Renal and systemic pH imaging by contrast-enhanced MRI. *Magn. Reson. Med.* **2003**, *49*, 249–257. (c) Kálmán, F. K.; Woods, M.; Caravan, P.; Jurek, P.; Spiller, M.; Tircso, G.; Kiraly, R.; Brücher, E.; Sherry, A. D. Potentiometric and Relaxometric Properties of Gadolinium-based MRI Contrast Agent for Sensing Tissue pH. *Inorg. Chem.* **2007**, *46*, 5260–5270.
- (6) Lowe, M. P.; Parker, D.; Reany, O.; Aime, S.; Botta, M.; Castellano, G.; Gianolio, E.; Pagliarin, R. pH-dependent modulation of relaxivity and luminescence in macrocyclic gadolinium and europium complexes based on reversible intramolecular sulfonamide ligation. *J. Am. Chem. Soc.* **2001**, *123*, 7601–7609.
- (7) Woods, M.; Kiefer, G. E.; Bott, S.; Castillo-Muzquiz, A.; Eshelbrenner, C.; Michaudet, L.; McMillan, K.; Mudigunda, S. D. K.; Ogrin, D.; Tircso, G.; Zhang, S.; Zhao, P.; Sherry, A. D. Synthesis, Relaxometric and Photophysical Properties of a New pH-Responsive MRI Contrast Agent: The Effect of Other Ligating Groups on Dissociation of a *p*-Nitrophenolic Pendant Arm. *J. Am. Chem. Soc.* **2004**, *126*, 9248–9256.
- (8) (a) Giovenzana, G. B.; Negri, R.; Rolla, G. A.; Tei, L. Gd-Aminoethyl-DO3A Complexes: A Novel Class of pH-Sensitive MRI Contrast Agents. *Eur. J. Inorg. Chem.* **2012**, *2012*, 2035–2039. (b) Baranyai, Z.; Rolla, G. A.; Negri, R.; Forgács, A.; Giovenzana, G. B.; Tei, L. Comprehensive Evaluation of the Physicochemical Properties of Ln^{III} Complexes of Aminoethyl-DO3A as pH-Responsive T₁-MRI Contrast Agents. *Chem. - Eur. J.* **2014**, *20*, 2933–2944.
- (9) Hall, J.; Haner, R.; Aime, S.; Botta, M.; Faulkner, S.; Parker, D.; de Sousa, A. S. Relaxometric and luminescence behaviour of triaqua-hexaazamacrocyclic complexes, the gadolinium complex displaying a high relaxivity with a pronounced pH dependence. *New J. Chem.* **1998**, *22*, 627–631.
- (10) de Leon-Rodriguez, L. M.; Lubag, A. J. M.; Malloy, C. R.; Martinez, G. V.; Gillies, R. J.; Sherry, A. D. Responsive MRI agents for sensing metabolism *in vivo*. *Acc. Chem. Res.* **2009**, *42*, 948–957.
- (11) Garcia-Martin, M. L.; Martinez, G. V.; Raghunand, N.; Sherry, A. D.; Zhang, S.; Gillies, R. J. High resolution pH(e) imaging of rat glioma using pH-dependent relaxivity. *Magn. Reson. Med.* **2006**, *55*, 309–315.
- (12) Aime, S.; Fedeli, F.; Sanino, A.; Terreno, E. R₂/R₁ Ratiometric Procedure for a Concentration-Independent, pH-Responsive, Gd(III)-Based MRI Agent. *J. Am. Chem. Soc.* **2006**, *128*, 11326–11327.
- (13) (a) Soesbe, T. C.; Wu, Y.; Sherry, A. D. Advantages of paramagnetic CEST complexes having slow-to-intermediate water exchange properties as responsive MRI agents. *NMR Biomed.* **2013**, *26*, 829–838. (b) Dorazio, S. J.; Olatunde, A. O.; Sperryak, J. A.; Morrow, J. R. CoCEST: cobalt(II) amide-appended paraCEST MRI contrast agents. *Chem. Commun.* **2013**, *49*, 10025–10027. (c) Sheth, V. R.; Li, Y.; Chen, L. Q.; Howison, C. M.; Flask, C. A.; Pagel, M. D. Measuring *in vivo* tumor pHe with CEST-FISP MRI. *Magn. Reson. Med.* **2012**, *67*, 760–768. (d) Liu, G.; Li, Y.; Sheth, V. R.; Pagel, M. D. Imaging *in vivo* extracellular pH with a single paramagnetic chemical exchange saturation transfer magnetic resonance imaging contrast agent. *Mol. Imaging* **2012**, *11*, 47–57. (e) Castelli, D. D.; Ferrauto, G.; Cutrin, J. C.; Terreno, E.; Aime, S. *In vivo* maps of extracellular pH in murine melanoma by CEST-MRI. *Magn. Reson. Med.* **2014**, *71*, 326–332.
- (14) Aime, S.; Castelli, D. D.; Terreno, E. Novel pH-reporter MRI contrast agents. *Angew. Chem., Int. Ed.* **2002**, *41*, 4334–4336.
- (15) Krchová, T.; Gálisová, A.; Jiráček, D.; Hermann, P.; Kotek, J. Ln(III)-complexes of a DOTA analogue with an ethylenediamine pendant arm as pH-responsive PARACEST contrast agents. *Dalton Trans.* **2016**, *45*, 3486–3496.
- (16) Castelli, D. D.; Terreno, E.; Aime, S. YbIII-HPDO3A: A Dual pH- and Temperature-Responsive CEST Agent. *Angew. Chem.* **2011**, *123*, 1838–1840.
- (17) Posse, S.; Otazo, R.; Dager, S. R.; Alger, J. MR spectroscopic imaging: principles and recent advances. *J. Magn. Reson. Imaging.* **2013**, *37*, 1301–1325.
- (18) Griffiths, R. J. Are cancer cells acidic? *Br. J. Cancer* **1991**, *64*, 425–427.
- (19) Gillies, R. J.; Morse, D. L. *In vivo* magnetic resonance spectroscopy in cancer. *Annu. Rev. Biomed. Eng.* **2005**, *7*, 287–326.
- (20) (a) van Sluis, R.; Bhujwalla, Z. M.; Raghunand, N.; Ballesteros, P.; Alvarez, J.; Cerdan, S.; Galons, J. P.; Gillies, R. J. *In vivo* imaging of extracellular pH using ¹H MRSI. *Magn. Reson. Med.* **1999**, *41*, 743–750. (b) Garcia-Martin, M. L.; Herigault, G.; Remy, C.; Farion, R.; Ballesteros, P.; Coles, J. A.; Cerdan, S.; Ziegler, A. Mapping Extracellular pH in Rat Brain Gliomas *In Vivo* by H Magnetic Resonance Spectroscopic Imaging: Comparison with Maps of Metabolites. *Cancer Res.* **2001**, *61*, 6524–6531.
- (21) Aime, S.; Botta, M.; Milone, L.; Terreno, E. Paramagnetic complexes as novel NMR pH indicators. *Chem. Commun.* **1996**, 1265–1266.
- (22) Coman, D.; Trubel, H. K.; Rycyna, R. E.; Hyder, F. Brain temperature and pH measured by (1)H chemical shift imaging of a thulium agent. *NMR Biomed.* **2009**, *22*, 229–239.
- (23) Huang, Y.; Coman, D.; Ali, M. M.; Hyder, F. Lanthanide ion (III) complexes of 1,4,7,10-tetraazacyclododecane-1,4,7,10-tetraaminophosphonate (DOTA-4AmP⁸⁻) for dual biosensing of pH with CEST (chemical exchange saturation transfer) and BIRDS (biosensor imaging of redundant deviation in shifts). *Contrast Media Mol. Imaging* **2015**, *10*, 51–58.
- (24) Jagadish, B.; Brickert-Albrecht, G. L.; Nichol, G. S.; Mash, E. A.; Raghunand, N. On the Synthesis of 1,4,7-Tris(tert-butoxycarbonylmethyl)-1,4,7,10-tetraazacyclododecane. *Tetrahedron Lett.* **2011**, *52*, 2058–2061.
- (25) Jiang, X.-J.; Lo, P.-Ch; Tsang, Y.-M.; Yeung, S.-L.; Fong, W.-P.; Ng, D. K. P. Phthalocyanine–Polyamine Conjugates as pH-Controlled

Photosensitizers for Photodynamic Therapy. *Chem. - Eur. J.* **2010**, *16*, 4777–4783.

(26) Perrin, D. D.; Armarego, W. L. F. *Purification of Laboratory Chemicals*, 3rd ed.; Pergamon Press: Oxford, 1988.

(27) *MATLAB R2015b*; The MathWorks Inc.: Natick, MA, 2000.

(28) Corsi, D. M.; Platas-Iglesias, C.; van Bekkum, H.; Peters, J. A. Determination of paramagnetic lanthanide (III) concentrations from bulk magnetic susceptibility shifts in NMR spectra. *Magn. Reson. Chem.* **2001**, *39*, 723–726.

(29) Sheldrick, G. M. *SHELXS97, Program for Crystal Structure Solution from Diffraction Data*; University of Göttingen: Göttingen, Germany, 1997.

(30) Sheldrick, G. M. *SHELXL97, Program for Crystal Structure Refinement from Diffraction Data*; University of Göttingen: Göttingen, Germany, 1997.

(31) (a) Táborský, P.; Lubal, P.; Havel, J.; Kotek, J.; Hermann, P.; Lukeš, I. Thermodynamic and Kinetic Studies of Lanthanide(III) Complexes with H₅do3ap (1,4,7,10-Tetraazacyclododecane-1,4,7-triacetic-10-(methylphosphonic Acid)), a Monophosphonate Analogue of H₄dota. *Collect. Czech. Chem. Commun.* **2005**, *70*, 1909–1942. (b) Försterová, M.; Svobodová, I.; Lubal, P.; Táborský, P.; Kotek, J.; Hermann, P.; Lukeš, I. Thermodynamic study of lanthanide(III) complexes with bifunctional monophosphinic acid analogues of H₄dota and comparative kinetic study of yttrium(III) complexes. *Dalton Trans.* **2007**, 535–549.

(32) Kývala, M.; Lukeš, I. *International Conference Chemometrics 95*; Pardubice, Czech Republic, 1995; p 63. Full version of *OPIUM* available (free of charge) on <http://web.natur.cuni.cz/~kyvala/opium.html>.

(33) Martell, A. E.; Smith, R. M.; Motekaitis, R. J. *NIST Critically Selected Stability Constants of Metal Complexes (Version 7)*; Texas A&M University: College Station, TX.

(34) Aime, S.; Botta, M.; Ermondi, G. NMR study of solution structures and dynamics of lanthanide(III) complexes of DOTA. *Inorg. Chem.* **1992**, *31*, 4291–4299.

(35) (a) Caravan, P.; Ellison, J. J.; McMurry, T. J.; Lauffer, R. B. Gadolinium(III) Chelates as MRI Contrast Agents: Structure, Dynamics, and Applications. *Chem. Rev.* **1999**, *99*, 2293–2352. (b) Hermann, P.; Kotek, J.; Kubíček, V.; Lukeš, I. Gadolinium(III) complexes as MRI contrast agents: ligand design and properties of the complexes. *Dalton Trans.* **2008**, 3027–3047. (c) Geraldes, C. F. G. C.; Laurent, S. Classification and basic properties of contrast agents for magnetic resonance imaging. *Contrast Media Mol. Imaging* **2009**, *4*, 1–23.

(36) (a) Aime, S.; Botta, M.; Fasano, M.; Marques, M. P. M.; Geraldes, C. F. G. C.; Pubanz, D.; Merbach, A. E. Conformational and Coordination Equilibria on DOTA Complexes of Lanthanide Metal Ions in Aqueous Solution Studied by (1)H-NMR Spectroscopy. *Inorg. Chem.* **1997**, *36*, 2059–2068. (b) Lebedušková, P.; Hermann, P.; Helm, L.; Tóth, E.; Kotek, J.; Binnemans, K.; Rudovský, J.; Lukeš, I.; Merbach, A. E. Gadolinium(III) Complexes of Mono- and Diethyl Esters of Monophosphonic Acid Analogue of DOTA as Potential MRI Contrast Agents: Solution Structures and Relaxometric Studies. *Dalton Trans.* **2007**, 493–501. (c) Vitha, T.; Kubíček, V.; Kotek, J.; Hermann, P.; Vander Elst, L.; Muller, R. N.; Lukeš, I.; Peters, J. A. Gd(III) complex of a monophosphinate-bis(phosphonate) DOTA analogue with a high relaxivity; Lanthanide(III) complexes for imaging and radiotherapy of calcified tissues. *Dalton Trans.* **2009**, 3204–3214. (d) Castelli, D. D.; Caligara, M. C.; Botta, M.; Terreno, E.; Aime, S. Combined high resolution NMR and H-1 and O-17 relaxometric study sheds light on the solution structure and dynamics of the Lanthanide(III) complexes of HPDO3A. *Inorg. Chem.* **2013**, *52*, 7130–7138. (e) Rudovský, J.; Cígler, P.; Kotek, J.; Hermann, P.; Vojtíšek, P.; Lukeš, I.; Peters, J. A.; Vander Elst, L.; Muller, R. N. Lanthanide (III) complexes of a mono (methylphosphonate) analogue of H₄dota: The influence of protonation of the phosphonate moiety on the TSAP/SAP isomer ratio and the water exchange rate. *Chem. - Eur. J.* **2005**, *11*, 2373–2384. (f) Rudovský, J.; Kotek, J.; Hermann, P.; Lukeš, I.; Mainero, V.; Aime, S. Synthesis of a Bifunctional

Monophosphinic Acid DOTA Analogue Ligand and Its Lanthanide-(III) Complexes. A Gadolinium(III) Complex Endowed with an Optimal Water Exchange Rate for MRI Applications. *Org. Biomol. Chem.* **2005**, *3*, 112–117.

(37) Krchová, T.; Kotek, J. Unpublished results.

(38) Beeby, A.; Clarkson, I. M.; Dickins, R. S.; Faulkner, S.; Parker, D.; Royle, L.; de Sousa, A. S.; Williams, J. A. G.; Woods, M. Non-radiative deactivation of the excited states of europium, terbium and ytterbium complexes by proximate energy-matched OH, NH and CH oscillators: an improved luminescence method for establishing solution hydration states. *J. Chem. Soc., Perkin Trans. 2* **1999**, 493–504.

(39) (a) Rudovský, J.; Botta, M.; Hermann, P.; Koridze, A.; Aime, S. Relaxometric and solution NMR structural studies on ditopic lanthanide(III) complexes of a phosphinate analogue of DOTA with a fast rate of water exchange. *Dalton Trans.* **2006**, 2323–2333. (b) Kotková, Z.; Pereira, G. A.; Djanashvili, K.; Kotek, J.; Rudovský, J.; Hermann, P.; Vander Elst, L.; Muller, R. N.; Geraldes, C. F. G. C.; Lukeš, I.; Peters, J. A. Lanthanide(III) Complexes of Phosphorus Acid Analogues of H₄DOTA as Model Compounds for the Evaluation of the Second-Sphere Hydration. *Eur. J. Inorg. Chem.* **2009**, 2009, 119–136. (c) Pereira, G. A.; Ball, L.; Sherry, A. D.; Peters, J. A.; Geraldes, C. F. G. C. NMR Characterization of Lanthanide(3+) Complexes of Tetraazatetrakisphosphinato and Tetraazatetrakisphosphonato Ligands. *Helv. Chim. Acta* **2009**, *92*, 2532–2551. (d) Rohovec, J.; Lukeš, I.; Hermann, P. Lanthanide complexes of a cyclen derivative with phenylphosphinic pendant arms for possible ¹H and ³¹P MRI temperature sensitive probes. *New J. Chem.* **1999**, *23*, 1129–1132. (e) Rohovec, J.; Kývala, M.; Vojtíšek, P.; Hermann, P.; Lukeš, I. Synthesis, Crystal Structures, and Solution Properties of *N*-Methylene-(phenyl)phosphinic Acid Derivatives of Cyclen and Cyclam. *Eur. J. Inorg. Chem.* **2000**, 2000, 195–203. (f) Aime, S.; Batsanov, A. S.; Botta, M.; Howard, J. A. K.; Parker, D.; Senanayake, K.; Williams, J. A. G. Solution and Solid-state Characterization of Highly Rigid, Eight-Coordinate Lanthanide(III) Complexes of a Macrocyclic Tetrabenzylphosphinate. *Inorg. Chem.* **1994**, *33*, 4696–4706. (g) Aime, S.; Batsanov, A. S.; Botta, M.; Dickins, R. S.; Faulkner, S.; Foster, C. E.; Harrison, A.; Howard, J. A. K.; Moloney, J. M.; Norman, T. J.; Parker, D.; Royle, L.; Williams, J. A. G. Nuclear magnetic resonance, luminescence and structural studies of lanthanide complexes with octadentate macrocyclic ligands bearing benzylphosphinate groups. *J. Chem. Soc., Dalton Trans.* **1997**, 3623–3636.

(40) Campello, M. P. C.; Lacerda, S.; Santos, I. C.; Pereira, G. A.; Geraldes, C. F. G. C.; Kotek, J.; Hermann, P.; Vaněk, J.; Lubal, P.; Kubíček, V.; Tóth, E.; Santos, I. Lanthanide(III) complexes of 4,10-bis(phosphonomethyl)-1,4,7,10-tetraazacyclododecane-1,7-diacetic acid (trans-H₆do2a2p) in solution and in the solid state: structural studies along the series. *Chem. - Eur. J.* **2010**, *16*, 8446–8465.

(41) (a) Blackburn, O. A.; Edkins, R. M.; Faulkner, S.; Kenwright, A. M.; Parker, D.; Rogers, N. J.; Shuvaev, S. Electromagnetic susceptibility anisotropy and its importance for paramagnetic NMR and optical spectroscopy in lanthanide coordination chemistry. *Dalton Trans.* **2016**, 45, 6782–6800. (b) Cucinotta, G.; Perfetti, M.; Luzon, J.; Etienne, M.; Car, P.-E.; Caneschi, A.; Calvez, G.; Bernot, K.; Sessoli, R. Magnetic Anisotropy in a Dysprosium/DOTA Single-Molecule Magnet: Beyond Simple Magneto-Structural Correlations. *Angew. Chem., Int. Ed.* **2012**, *51*, 1606–1610.

(42) (a) Rohovec, J.; Vojtíšek, P.; Hermann, P.; Mosinger, J.; Žák, Z.; Lukeš, I. Synthesis, crystal structures and NMR and luminescence spectra of lanthanide complexes of 1,4,7,10-tetraazacyclododecane with *N*-methylene(phenyl)phosphinic acid pendant arms. *J. Chem. Soc., Dalton Trans.* **1999**, 3585–3592. (b) Avcilla, F.; Peters, J. A.; Geraldes, C. F. G. C. X-ray Crystal Structure of a Sodium Salt of [Gd(DOTP)]⁵⁻: Implications for Its Second-Sphere Relaxivity and the ²³Na NMR Hyperfine Shift Effects of [Tm(DOTP)]⁵⁻. *Eur. J. Inorg. Chem.* **2003**, 2003, 4179–4186. (c) Vojtíšek, P.; Cígler, P.; Kotek, J.; Rudovský, J.; Hermann, P.; Lukeš, I. Crystal Structures of Lanthanide-(III) Complexes with Cyclen Derivative Bearing Three Acetate and One Methylphosphonate Pendants. *Inorg. Chem.* **2005**, *44*, 5591–5599. (d) Luck, R. L.; Maupin, C. L.; Parker, D.; Riehl, J. P.; Williams,

J. A. G. Circularly polarized luminescence and structural studies of a dysprosium(III) complex with an octadentate macrocyclic ligand bearing benzylphosphinate groups. *Inorg. Chim. Acta* **2001**, *317*, 331–337.

(43) Lukeš, I.; Kotek, J.; Vojtíšek, P.; Hermann, P. Tetraazacycles with Methylphosphinic/phosphonic Acid Pendant Arms. A Comparison with their Acetic Acid Analogues. *Coord. Chem. Rev.* **2001**, *216–217*, 287–312.

(44) Krchová, T.; Kotek, J.; Jiráček, D.; Havlíčková, J.; Čiřářová, I.; Hermann, P. Lanthanide(III) complexes of aminoethyl-DO3A as PARACEST contrast agents based on decoordination of the weakly bound amino group. *Dalton Trans.* **2013**, *42*, 15735–15747.

(45) Pniok, M.; Kubíček, V.; Havlíčková, J.; Kotek, J.; Sabatie-Gogova, A.; Plutnar, J.; Huclier-Markai, S.; Hermann, P. Thermodynamic and kinetic study of scandium(III) complexes of DTPA and DOTA: a step toward scandium radiopharmaceuticals. *Chem. - Eur. J.* **2014**, *20*, 7944–7955.